

Complementarity of LHC and EDMs for Exploring Higgs CP Violation

Chien-Yi Chen,^a S. Dawson^a and Yue Zhang^b

^a*Department of Physics, Brookhaven National Laboratory,
Upton, New York, 11973*

^b*Walter Burke Institute for Theoretical Physics, California Institute of Technology,
Pasadena, CA 91125*

E-mail: cychen@bnl.gov, dawson@bnl.gov, yuezhang@caltech.edu

ABSTRACT: We analyze the constraints on a CP-violating, flavor conserving, two Higgs doublet model from the measurements of Higgs properties and from the search for heavy Higgs bosons at LHC, and show that the stronger limits typically come from the heavy Higgs search channels. The limits on CP violation arising from the Higgs sector measurements are complementary to those from EDM measurements. Combining all current constraints from low energy to colliders, we set generic upper bounds on the CP violating angle which parametrizes the CP odd component in the 126 GeV Higgs boson.

Contents

1	Introduction	1
2	Two Higgs Doublet Models and CP Violation	3
2.1	Scalar Potential with Two Higgs Doublets	3
2.2	Neutral Scalar Interactions	4
2.3	CP Violation Implies a Non-Decoupled Heavy Higgs Sector	4
2.4	Beyond Approximate Z_2 Symmetry	6
2.5	Production and Decay of the Heavy Higgs at LHC	6
2.5.1	Production	6
2.5.2	Decays	7
2.6	CP violation and Heavy Higgs Signal Rates	9
3	Results	11
3.1	Limits from Heavy Higgs Searches in Approximate Z_2 Symmetric Models	12
3.2	Limits from Heavy Higgs Searches in the Models with no Z_2 Symmetry	15
4	Limits from B Decays, Oblique Parameters, and $(g - 2)_\mu$	22
4.1	Limits from Electroweak Oblique Parameters	22
4.2	Limits from muon $g - 2$	24
5	Conclusion	26
A	Solving the potential parameters in the approximate Z_2 case	27
B	Tri-linear Higgs Couplings	27
C	Formula for $g - 2$	28

1 Introduction

Now that the 126 GeV Higgs boson has been discovered [1, 2], the exploration of its properties is the focus of LHC phenomenology. The current measurements of Higgs production and decay rates are consistent with the Standard Model (SM) predictions at the $\sim 10 - 20\%$ level, leaving open the possibility that there is additional physics in the Higgs sector. One attractive alternative to the SM is the two Higgs doublet model (2HDM), which has 5 Higgs bosons, allowing for new phenomena in the Higgs sector [3]. The couplings of the Higgs bosons to fermions and gauge bosons in the CP conserving 2HDM depend on 2 parameters: α , which

describes the mixing in the neutral Higgs boson sector, and $\tan\beta$, the ratio of Higgs vacuum expectation values. Measurements of Higgs coupling properties in the CP conserving limit require that the 2HDM be close to the alignment limit, $\beta - \alpha \sim \frac{\pi}{2}$ [4–7].

The SM explains CP violation through the CKM mixing matrix, which is sufficient to account for observed CP violation in the B and K systems. However, it is insufficient to explain the excess of matter over anti-matter in the universe, suggesting that there may be further sources of CP violation [8, 9]. The 2HDM offers the possibility for a new source of CP violation beyond the CKM matrix and QCD θ term. In such a scenario, the 126 GeV Higgs boson can be a mixture of CP even and CP odd states [10–14]. The LHC data has already excluded the case that the 126 Higgs is a pure CP odd scalar [15, 16], but the constraints on its CP odd mixture are still rather weak. There have been proposals of new techniques to directly measure the Higgs CP mixture in future colliders [17–24]. The parameters of the CP violating version of the 2HDM receive complementary limits from LHC Higgs coupling measurements and from low energy measurements such as electric dipole moments (EDMs). The measurements of Higgs couplings do not put a strong constraint on the CP violating phase, especially in the alignment limit [10], and the strongest limits come from EDMs [8, 10, 11, 25–27].

CP violation in the Higgs sector has been studied extensively in the MSSM limit of the 2HDM [28, 29]. The MSSM contains many sources of CP violation from the soft SUSY breaking terms in the effective Lagrangian [30]. The primary restriction on this type of CP violation arises from the requirement that the lightest Higgs boson have a mass near 126 GeV [31]. Analogous limits to those obtained in this work from Higgs couplings, heavy Higgs searches, and EDMs can be found in the MSSM [32, 33].

We consider a CP violating 2HDM scenario which has a softly broken Z_2 symmetry which avoids large flavor changing neutral currents from Higgs exchange, but allows for new CP violation from the scalar potential. We further allow the Higgs couplings to have small deviations from the alignment limit. In this work, we consider the additional constraints on the parameters of the theory arising from the search for heavy Higgs bosons. In the CP conserving 2HDM, the search for heavy Higgs bosons significantly restricts the allowed parameter space for small $\tan\beta$ [34, 35] and this remains true in the CP violating case. In the context of the 2HDMs, if there is significant CP violation, the heavy Higgs boson masses cannot be too heavy and in some regions of parameter space the LHC heavy Higgs searches can place the leading constraint on CP violation.

In Section 2, we review the CP violating 2HDM and predictions for Higgs boson production and decay within this class of models. Limits from heavy Higgs searches are discussed in Section 3 and compared with low energy limits from the electron EDM. We have also updated the results of Refs. [10, 36–38] for the limits on the CP violating parameters from Higgs coupling fits. Finally, Section 5 contains a concluding discussion of the complementary limits on CP violating 2HDMs from Higgs coupling fits, heavy Higgs searches, EDMs, the oblique parameters, and $g - 2$.

2 Two Higgs Doublet Models and CP Violation

In this section we review the 2HDMs considered in this study.

2.1 Scalar Potential with Two Higgs Doublets

The most general two Higgs doublet potential which breaks $SU(2)_L \times U(1)$ to $U(1)_{EM}$ is,

$$\begin{aligned}
V(\phi_1, \phi_2) = & -\frac{1}{2} \left[m_{11}^2 (\phi_1^\dagger \phi_1) + \left(m_{12}^2 (\phi_1^\dagger \phi_2) + \text{h.c.} \right) + m_{22}^2 (\phi_2^\dagger \phi_2) \right] \\
& + \frac{\lambda_1}{2} (\phi_1^\dagger \phi_1)^2 + \frac{\lambda_2}{2} (\phi_2^\dagger \phi_2)^2 + \lambda_3 (\phi_1^\dagger \phi_1) (\phi_2^\dagger \phi_2) + \lambda_4 (\phi_1^\dagger \phi_2) (\phi_2^\dagger \phi_1) \\
& + \frac{1}{2} \left[\lambda_5 (\phi_1^\dagger \phi_2)^2 + \lambda_6 (\phi_1^\dagger \phi_2) (\phi_1^\dagger \phi_1) + \lambda_7 (\phi_1^\dagger \phi_2) (\phi_2^\dagger \phi_2) + \text{h.c.} \right]. \quad (2.1)
\end{aligned}$$

The potential of Eq. (2.1) leads to tree level flavor changing neutral currents, which can be avoided by imposing a Z_2 symmetry under which,

$$\phi_1 \rightarrow -\phi_1 \quad \phi_2 \rightarrow \phi_2. \quad (2.2)$$

Eq. (2.2) implies $\lambda_6 = \lambda_7 = 0$, while a non-zero m_{12} softly breaks the Z_2 symmetry of Eq. (2.2).

After electroweak symmetry breaking, the Higgs doublets in unitary gauge can be written as,

$$\phi_1 = \begin{pmatrix} -\sin \beta H^+ \\ \frac{1}{\sqrt{2}}(v \cos \beta + H_1^0 - i \sin \beta A^0) \end{pmatrix}, \quad \phi_2 = e^{i\xi} \begin{pmatrix} \cos \beta H^+ \\ \frac{1}{\sqrt{2}}(v \sin \beta + H_2^0 + i \cos \beta A^0) \end{pmatrix}, \quad (2.3)$$

where $\tan \beta = v_2/v_1$, $v = \sqrt{|v_1|^2 + |v_2|^2} = 246$ GeV and H^+ is the physical charged Higgs with mass m_{H^+} . We are free to redefine fields and go to a basis where $\xi = 0$. In general there are 2 independent phases and the imaginary parts of m_{12} and λ_5 lead to mixing in the neutral Higgs sector between H_1^0, H_2^0 and A^0 , and that is the source of CP violation.

The mixing among the three neutral scalars can be parametrized by an orthogonal matrix R ,

$$R = \begin{pmatrix} -s_\alpha c_{\alpha_b} & c_\alpha c_{\alpha_b} & s_{\alpha_b} \\ s_\alpha s_{\alpha_b} s_{\alpha_c} - c_\alpha c_{\alpha_c} & -s_\alpha c_{\alpha_c} - c_\alpha s_{\alpha_b} s_{\alpha_c} & c_{\alpha_b} s_{\alpha_c} \\ s_\alpha s_{\alpha_b} c_{\alpha_c} + c_\alpha s_{\alpha_c} & s_\alpha s_{\alpha_c} - c_\alpha s_{\alpha_b} c_{\alpha_c} & c_{\alpha_b} c_{\alpha_c} \end{pmatrix}. \quad (2.4)$$

where $s_\alpha = \sin \alpha$, etc and

$$-\frac{\pi}{2} < \alpha_b \leq \frac{\pi}{2} \quad -\frac{\pi}{2} \leq \alpha_c \leq \frac{\pi}{2}. \quad (2.5)$$

The physical mass eigenstates are then defined as $(h_1, h_2, h_3)^T = R(H_1^0, H_2^0, A^0)^T$. In the CP conserving version of the 2HDM, $\alpha_b = \alpha_c = 0$, R is block diagonal, and h_1 and h_2 have no pseudoscalar component.

2.2 Neutral Scalar Interactions

For simplicity, we focus on the 2HDMs where the Yukawa sector has a Z_2 symmetry and ϕ_1 and ϕ_2 each only gives mass to up or down type fermions. This is sufficient to suppress tree-level flavor changing processes mediated by the neutral Higgs scalars. For the 3rd generation (and suppressing CKM mixing),

$$\mathcal{L} = \begin{cases} -\left(\frac{\cos \alpha}{\sin \beta} \frac{m_t}{v}\right) \bar{Q}_L (i\tau_2) \phi_2^* t_R - \left(\frac{\cos \alpha}{\sin \beta} \frac{m_b}{v}\right) \bar{Q}_L \phi_2 b_R + \text{h.c.} & \text{Type I} \\ -\left(\frac{\cos \alpha}{\sin \beta} \frac{m_t}{v}\right) \bar{Q}_L (i\tau_2) \phi_2^* t_R + \left(\frac{\sin \alpha}{\cos \beta} \frac{m_b}{v}\right) \bar{Q}_L \phi_1 b_R + \text{h.c.} & \text{Type II,} \end{cases} \quad (2.6)$$

where $Q_L^T = (t_L, b_L)$. In both cases, we assume that the charged lepton Yukawa coupling has the same form as that of the charge $-1/3$ quarks. Under the Z_2 symmetry, Q_L, t_R, ϕ_2 are always even, ϕ_1 is always odd, and b_R is even (odd) in Type I (II) models.

From this we can derive the couplings between neutral Higgs bosons and the fermions and gauge bosons. As a general parametrization we take,

$$\mathcal{L} = \sum_{i=1}^3 \left[-m_f (c_{f,i} \bar{f} f + \tilde{c}_{f,i} \bar{f} i \gamma_5 f) \frac{h_i}{v} + (2a_i M_W^2 W_\mu W^\mu + a_i M_Z^2 Z_\mu Z^\mu) \frac{h_i}{v} \right]. \quad (2.7)$$

When $c_{f,i} \tilde{c}_{f,i} \neq 0$ or $a_i \tilde{c}_{f,i} \neq 0$, the mass eigenstate h_i couples to both CP even and CP odd operators, so the theory violates CP. The coefficients $c_{f,i}$, $\tilde{c}_{f,i}$ and a_i can be derived from $\tan \beta$ and the elements of the matrix R defined above. An appealing feature is that all couplings

	$c_{t,i}$	$c_{b,i} = c_{\tau,i}$	$\tilde{c}_{t,i}$	$\tilde{c}_{b,i} = \tilde{c}_{\tau,i}$	a_i
Type I	$R_{i2}/\sin \beta$	$R_{i2}/\sin \beta$	$-R_{i3} \cot \beta$	$R_{i3} \cot \beta$	$R_{i2} \sin \beta + R_{i1} \cos \beta$
Type II	$R_{i2}/\sin \beta$	$R_{i1}/\cos \beta$	$-R_{i3} \cot \beta$	$-R_{i3} \tan \beta$	$R_{i2} \sin \beta + R_{i1} \cos \beta$

Table 1. Fermion and gauge boson couplings to Higgs mass eigenstates.

in Table 1 depend on only four parameters, α , α_b , α_c and $\tan \beta$. It is worth noting that the couplings of the light Higgs boson h_1 to the gauge bosons and fermions are independent of α_c . Fits to the CP conserving 2HDM suggest that the couplings are close to the alignment limit, $\beta - \alpha \sim \frac{\pi}{2}$, implying that h_1 has couplings very close to the SM predictions. In our numerical studies, we will allow small deviations from the alignment limit.

2.3 CP Violation Implies a Non-Decoupled Heavy Higgs Sector

In general, the imposed Z_2 symmetry in the Yukawa sector is not preserved by renormalization. The hard breaking λ_6, λ_7 terms from the Higgs potential will induce couplings of ϕ_1, ϕ_2 to both up and down type quarks. This does not reintroduce any tree level flavor changing effects because the induced Yukawa matrices are still aligned with the corresponding fermion mass matrices. Motivated by this, a convenient choice is to forbid the λ_6, λ_7 terms. In this

case, the model has an approximate Z_2 symmetry, which is only softly broken by the m_{12}^2 term.

For the approximate Z_2 symmetric model, all of the potential parameters can be solved for in terms of the following parameters:

- The scalar masses, m_{h_1} , m_{h_2} , m_{h_3} and m_{H^\pm}
- The neutral scalar mixing angles, α , α_b , α_c
- The ratio of vev's, $\tan \beta$
- One potential parameter, $\text{Re}(m_{12}^2)$, or $\nu \equiv \text{Re}(m_{12})^2/(v^2 \sin 2\beta)$,

giving 9 physical parameters. The ν parameter controls the decoupling limit, *i.e.*, when $\text{Re}(m_{12})^2$ approaches infinity, the masses of h_2 , h_3 and H^\pm also go to infinity.

The explicit solution for the parameters of the scalar potential was found in Ref. [10], and is listed below in Appendix A. The imaginary part of λ_5 , which is a source of CP violation, is given by,

$$\text{Im}\lambda_5 = \frac{2 \cos \alpha_b}{v^2 \sin \beta} \left[(m_{h_2}^2 - m_{h_3}^2) \cos \alpha \sin \alpha_c \cos \alpha_c + (m_{h_1}^2 - m_{h_2}^2 \sin^2 \alpha_c - m_{h_3}^2 \cos^2 \alpha_c) \sin \alpha \sin \alpha_b \right] . \quad (2.8)$$

An important point here is that, in order for the 126 GeV Higgs boson to have CP violating couplings, the heavy Higgs states must not decouple. Otherwise, the two Higgs doublet model will return to the SM limit. This is actually our main motivation for studying the bounds on the non-decoupled heavy Higgs.

Clearly, when the scalars $h_{2,3}$ are much heavier than the electroweak scale, and $m_{h_2} \simeq m_{h_3} \equiv m_{H^+} \gg m_{h_1}$,

$$|\sin 2\alpha_b| \simeq \frac{|\text{Im}\lambda_5| v^2}{m_{H^+}^2} \left| \frac{\sin \beta}{\sin \alpha} \right| . \quad (2.9)$$

The unitarity bound on $\text{Im}\lambda_5$, $\text{Im}\lambda_5 < 4\pi$, sets the largest allowed CP violating mixing angle α_b . This implies that for an $\mathcal{O}(1)$ $\sin \alpha_b$ to be theoretically accessible, the heavy scalars h_2 , h_3 and H^\pm must be not far above the electroweak scale. In general, for nonzero α_b , the masses of the heavy scalars should satisfy

$$m_{H^+} \lesssim 870 \text{ GeV} \times \sqrt{|\text{Im}\lambda_5|/(4\pi)} \sqrt{|\sin \beta/(\sin \alpha \sin 2\alpha_b)|} . \quad (2.10)$$

A similar conclusion holds when one goes beyond the approximate Z_2 symmetry by including the λ_6, λ_7 terms.

2.4 Beyond Approximate Z_2 Symmetry

For the approximate Z_2 symmetric model, there is a further theoretical constraint on the physical parameters resulting from the minimization of the potential. This constraint is given in Eq. (A.10) and can be transformed into a quadratic equation for $\tan \alpha_c$. The condition for α_c to have a real solution is

$$\sin^2 \alpha_b \leq \frac{(m_{h_3}^2 - m_{h_2}^2)^2 \cot^2(\alpha + \beta)}{4(m_{h_2}^2 - m_{h_1}^2)(m_{h_3}^2 - m_{h_1}^2)} \equiv \sin^2 \alpha_b^{\max}. \quad (2.11)$$

When Eq. (2.11) is satisfied, the solutions for α_c are,

$$\alpha_c = \begin{cases} \alpha_c^-, & \alpha + \beta \leq 0 \\ \alpha_c^+, & \alpha + \beta > 0 \end{cases}, \quad \tan \alpha_c^\pm = \frac{\mp |\sin \alpha_b^{\max}| \pm \sqrt{\sin^2 \alpha_b^{\max} - \sin^2 \alpha_b}}{\sin \alpha_b} \sqrt{\frac{m_{h_3}^2 - m_{h_1}^2}{m_{h_2}^2 - m_{h_1}^2}}. \quad (2.12)$$

Eq. (2.11) implies an additional theoretical upper bound on the CP violating angle α_b , when the other parameters are fixed. In practice, we sometimes find this bound can be stronger than all the experimental limits. However, this is only a bound because of theoretical prejudice. In fact, it can be removed with a minimal step beyond the approximate Z_2 symmetric case by introducing a λ_7 term, with λ_7 being purely imaginary. In this case, the bound Eq. (2.11) no longer exists, α_c becomes a free parameter, and $\text{Im}\lambda_7$ can in turn be solved for as,

$$\text{Im}\lambda_7 = \frac{2 \cos \alpha_b}{v^2 \tan^2 \beta} \left[(m_{h_3}^2 - m_{h_2}^2) \sin \alpha_c \cos \alpha_c \frac{\cos(\alpha + \beta)}{\cos^2 \beta} + (m_{h_2}^2 \sin^2 \alpha_c + m_{h_3}^2 \cos^2 \alpha_c - m_{h_1}^2) \sin \alpha_b \frac{\sin(\alpha + \beta)}{\cos^2 \beta} \right]. \quad (2.13)$$

Although introducing hard Z_2 breaking ($\lambda_{6,7} \neq 0$) makes the Yukawa structure in Eq. (2.6) unnatural, one might argue it is accidentally the case at the electroweak scale.¹ In the phenomenological study in the next section, we will give the results for both the approximate Z_2 case, and the minimal extension as discussed in this subsection.

2.5 Production and Decay of the Heavy Higgs at LHC

2.5.1 Production

The dominant heavy Higgs boson production channels relevant to this study are gluon fusion, $gg \rightarrow h_{2,3}$, vector boson fusion, $qq \rightarrow qqh_{2,3}$, and production in association with bottom quarks, $gg/q\bar{q} \rightarrow h_{2,3}b\bar{b}$. In the 2HDM we explore, the interactions between the heavy neutral

¹We are aware that allowing Z_2 breaking terms in the Yukawa sector can introduce additional sources of CP violation. The price for this is introducing tree level flavor changing effects at the same time, and some flavor alignment mechanism must be resorted to [39–41]. We do not consider such a possibility, but focus on CP violation only from the Higgs sector in this work.

Higgs bosons and the SM fermions and the W, Z gauge bosons are simply rescaled from those of a SM-like Higgs boson, H_{SM} , by a factor given in Table 1. Therefore, it is convenient to take the SM-like Higgs cross sections, and rescale them with these factors and the appropriate form factors. The LHC production cross sections for a heavy SM-like Higgs boson have been calculated by the LHC Higgs Cross Section Working Group and given in [42, 43].

For the gluon fusion process, we calculate the ratio of the heavy Higgs boson production cross section in a CP violating 2HDM to that of a SM-like Higgs with the same mass. At one-loop,

$$R_{gg}^i = \frac{\sigma(gg \rightarrow h_i)}{\sigma(gg \rightarrow H_{SM})} = \frac{\left| c_{t,i} A_{1/2}^H(\tau_t^i) + c_{b,i} A_{1/2}^H(\tau_b^i) \right|^2 + \left| \tilde{c}_{t,i} A_{1/2}^A(\tau_t^i) + \tilde{c}_{b,i} A_{1/2}^A(\tau_b^i) \right|^2}{\left| A_{1/2}^H(\tau_t^i) + A_{1/2}^H(\tau_b^i) \right|^2}, \quad (2.14)$$

where $\tau_f^i = m_{h_i}^2/(4m_f^2)$ and $i = 1, 2, 3$, $f = t, b$. The form factors $A_{1/2}^H, A_{1/2}^A$ are given by

$$A_{1/2}^H(\tau) = 2(\tau + (\tau - 1)f(\tau))\tau^{-2}, \quad (2.15)$$

$$A_{1/2}^A(\tau) = 2f(\tau)\tau^{-1}, \quad (2.16)$$

$$f(\tau) = \begin{cases} \arcsin^2(\sqrt{\tau}), & \tau \leq 1 \\ \frac{1}{4} \left[\log\left(\frac{1+\sqrt{1-\tau^{-1}}}{1-\sqrt{1-\tau^{-1}}}\right) - i\pi \right]^2, & \tau > 1 \end{cases}. \quad (2.17)$$

For vector boson fusion, the ratio of the heavy Higgs production cross section in a 2HDM to that of a SM-like Higgs with the same mass is simply

$$R_{VBF}^i = \frac{\sigma(qq \rightarrow qqh_i)}{\sigma(qq \rightarrow qqH_{SM})} = (a_i)^2. \quad (2.18)$$

For $h_{2,3}b\bar{b}$ associated production, we take the NLO cross section for SM-like Higgs boson production in the 4 flavor number scheme from Ref. [44, 45]. There the cross section contains two pieces, one is proportional to y_b^2 , and the other proportional to $y_b y_t$ from interference. We rescale these results with the heavy Higgs-fermion couplings in a 2HDM,

$$\sigma(b\bar{b} \rightarrow h_i) = (c_{b,i})^2 \sigma_b^H(m_{h_i}) + c_{t,i} c_{b,i} \sigma_t^H(m_{h_i}) + (\tilde{c}_{b,i})^2 \sigma_b^A(m_{h_i}) + \tilde{c}_{t,i} \tilde{c}_{b,i} \sigma_t^A(m_{h_i}), \quad (2.19)$$

where σ_b^H is the cross section for $gg \rightarrow b\bar{b}h_i$ where the Higgs couples to the b quarks, σ_t^H is the interference between diagrams contributing to $gg \rightarrow b\bar{b}h_i$ where the Higgs couples to the b and the t quark. σ_b^A and σ_t^A are the corresponding contributions from the pseudoscalar couplings to the b and t quarks given in Eq. (2.7). Results in the 5 flavor number scheme [46] are quite similar and do not affect our conclusions.

2.5.2 Decays

The heavy neutral scalar to electroweak gauge boson decay rates are

$$\Gamma(h_i \rightarrow VV) = (a_i)^2 \frac{G_F m_{h_i}^3}{16\sqrt{2}\pi} \delta_V \left(1 - \frac{4M_V^2}{m_{h_i}^2}\right)^{1/2} \left[1 - \frac{4M_V^2}{m_{h_i}^2} + \frac{3}{4} \left(\frac{4M_V^2}{m_{h_i}^2}\right)^2\right], \quad (2.20)$$

where $V = W, Z$ and $\delta_W = 2$, $\delta_Z = 1$, and $i = 2, 3$. We note that in the alignment limit, $\Gamma(h_{2,3} \rightarrow VV) = 0$ when $\sin \alpha_b = \sin \alpha_c = 0$. These channels open up with non-zero CP violation. The decay rates to SM fermions are

$$\Gamma(h_i \rightarrow \bar{f}f) = \left[(c_{f,i})^2 + (\tilde{c}_{f,i})^2 \right] \frac{N_c G_F m_f^2 m_{h_i}}{4\sqrt{2}\pi} \left(1 - \frac{4m_f^2}{m_{h_i}^2} \right)^{3/2}, \quad (2.21)$$

where $N_c = 3$ for quarks and 1 for charged leptons.

The heavy scalars can also decay to a pair of gluons via a loop of top or bottom quarks, and the rates are

$$\Gamma(h_i \rightarrow gg) = \frac{\alpha_s^2 G_F m_{h_i}^3}{64\sqrt{2}\pi^3} \left[\left| c_{t,i} A_{1/2}^H(\tau_t^i) + c_{b,i} A_{1/2}^H(\tau_b^i) \right|^2 + \left| \tilde{c}_{t,i} A_{1/2}^A(\tau_t^i) + \tilde{c}_{b,i} A_{1/2}^A(\tau_b^i) \right|^2 \right]. \quad (2.22)$$

Clearly a decay rate is a CP even quantity. Thus, in all the above decay rates, the CP even coefficient c_f^i and the CP odd one \tilde{c}_f^i always contribute incoherently.

In our study, we are also interested in the heavy neutral scalars, h_2, h_3 , decaying into the Z boson and the 126 GeV Higgs boson,

$$\begin{aligned} \Gamma(h_i \rightarrow Zh_1) &= \frac{|g_{iz1}|^2}{16\pi m_{h_i}^3} \sqrt{\left(m_{h_i}^2 - (m_{h_1} + M_Z)^2 \right) \left(m_{h_i}^2 - (m_{h_1} - M_Z)^2 \right)} \\ &\times \left[-2m_{h_i}^2 + 2m_{h_1}^2 - M_Z^2 + \frac{1}{M_Z^2} (m_{h_i}^2 - m_{h_1}^2)^2 \right], \end{aligned} \quad (2.23)$$

where $g_{iz1} = (e/\sin 2\theta_W) [(-\sin \beta R_{11} + \cos \beta R_{12})R_{i3} - (-\sin \beta R_{i1} + \cos \beta R_{i2})R_{13}]$.

We have also calculated the decay rate of $h_i \rightarrow 2h_1$ from the Higgs self-interactions. The decay rate is

$$\Gamma(h_i \rightarrow h_1 h_1) = \frac{g_{i11}^2 v^2}{2\pi m_{h_i}} \sqrt{1 - \frac{4m_{h_1}^2}{m_{h_i}^2}}, \quad (2.24)$$

where g_{i11} , ($i = 2, 3$) are defined in Appendix B.

To get the branching ratios, we calculate the total width of the heavy Higgs²,

$$\begin{aligned} \Gamma_{tot}(h_i) &= \Gamma(h_i \rightarrow W^+W^-) + \Gamma(h_i \rightarrow ZZ) + \Gamma(h_i \rightarrow t\bar{t}) + \Gamma(h_i \rightarrow b\bar{b}) \\ &+ \Gamma(h_i \rightarrow \tau^+\tau^-) + \Gamma(h_i \rightarrow gg) + \Gamma(h_i \rightarrow Zh_1) + \Gamma(h_i \rightarrow h_1 h_1). \end{aligned} \quad (2.25)$$

Finally, for each channel, the ratio of signal strengths in the 2HDM to the counterpart in the SM is given by,

$$\mu_i^{XX} = \frac{(\sigma_7^i \mathcal{L}_7 + \sigma_8^i \mathcal{L}_8) \times \text{Br}(h_i \rightarrow XX)}{(\sigma_7^{\text{SM}} \mathcal{L}_7 + \sigma_8^{\text{SM}} \mathcal{L}_8) \times \text{Br}^{\text{SM}}(h_i \rightarrow XX)}, \quad (2.26)$$

² The rate $h_i \rightarrow \gamma\gamma$ for $i = 2, 3$ is always small and can be neglected here.

where, for example, the production cross sections are given by

$$\sigma_7^i = \sigma_{gg,7} R_{gg}^i + \sigma_{VBF,7} R_{VBF}^i + \sigma_{VH,7} R_{VH}^i, \quad (2.27)$$

$\sigma_{gg,7}$ is the gluon fusion cross section from Ref. [42, 43] for a SM Higgs boson with a mass of m_{h_i} , and $\mathcal{L}_{7,8}$ are the luminosities used in the experimental analysis. With this quantity, we are able to reinterpret the constraints on a heavy SM-like Higgs boson for the heavy neutral scalars in the 2HDM.

2.6 CP violation and Heavy Higgs Signal Rates

At this point, it is useful to gain some intuition about the impact of CP violation on the heavy Higgs to gauge boson decay channels, $h_i \rightarrow VV$ and $h_i \rightarrow Zh_1$ with ($i = 2, 3$). It is convenient to redefine the Higgs doublets and go to a basis where only one doublet, called ϕ'_1 , gets the 246 GeV vev, while the other ϕ'_2 has no vev [13, 67].

We start from a special point in the parameter space where the lightest Higgs, h_1 , has exactly the same couplings does the SM Higgs boson. This corresponds to having the mixing angles in Eq. (2.4) satisfy $\alpha_b = \alpha_c = 0$, and $\beta - \alpha = \pi/2$. The Higgs sector preserves CP invariance at this point. In this case, h_1 is the excitation arising from ϕ'_1 defined above, while $h_{2,3}$ are excitations from ϕ'_2 . As a result, the decay rates $h_i \rightarrow VV$ and $h_i \rightarrow Zh_1$ both vanish for $i = 2, 3$. It is worth noticing that this special point can be approached without going to the real decoupling limit by sending the second doublet mass to infinity.

Next, we turn on CP violation by making $\alpha_b = 0.5$, but still keep $\alpha_c = 0$. Here we discuss an example by fixing $\tan \beta = 20$ (in the basis of $\{\phi_1, \phi_2\}$ given in Eq. (2.3)) and vary the angle α , or the quantity $\cos(\beta - \alpha)$. We also choose the heavy neutral scalar masses to be $m_{h_2} = 400$ GeV and $m_{h_3} = 450$ GeV. In Fig. 1, we plot the gluon fusion production cross section and the gauge boson branching ratios of $h_{2,3}$ as a function of $\cos(\beta - \alpha)$. There are several suppressed regions which can be understood from Table 1. In the case $\alpha_c = 0$, we have in the Type-I model,

$$\begin{aligned} c_{t,2} = c_{b,2} &= -\frac{\sin \alpha}{\sin \beta}, \quad \tilde{c}_{t,2} = -\tilde{c}_{b,2} = 0, \\ c_{t,3} = c_{b,3} &= -\frac{\cos \alpha}{\sin \beta} \sin \alpha_b, \quad \tilde{c}_{t,3} = -\tilde{c}_{b,3} = -\cos \alpha_b \cot \beta. \end{aligned} \quad (2.28)$$

First, the gluon fusion production cross section for h_2 via a top or bottom loop vanishes at $\alpha = 0$ (near $\cos(\beta - \alpha) \simeq 0$). In the example we describe here, $\beta = \arctan(20)$ is close to $\pi/2$, and $c_{t,2} = c_{b,2}$ vanishes at $\alpha = 0$. Second, at $\alpha = \pm\pi/2$, (near $\cos(\beta - \alpha) \simeq \pm 1$), the couplings $c_{t,3}$ and $c_{b,3}$ vanish. As a result, the production cross section for h_3 is suppressed because $\tilde{c}_{t,3}$ and $\tilde{c}_{b,3}$ are both suppressed by $\cot \beta = 1/20$ in this case. On the other hand, the gauge boson decays of $h_{2,3}$ are directly controlled by $\beta - \alpha$. We list the relevant couplings here, again for $\alpha_c = 0$,

$$\begin{aligned} a_2 &= -\cos(\beta - \alpha), \quad g_{2z1} = -\frac{e}{\sin 2\theta_W} \sin(\beta - \alpha) \sin \alpha_b \\ a_3 &= -\sin(\beta - \alpha) \sin \alpha_b, \quad g_{3z1} = \frac{e}{\sin 2\theta_W} \cos(\beta - \alpha), \end{aligned} \quad (2.29)$$

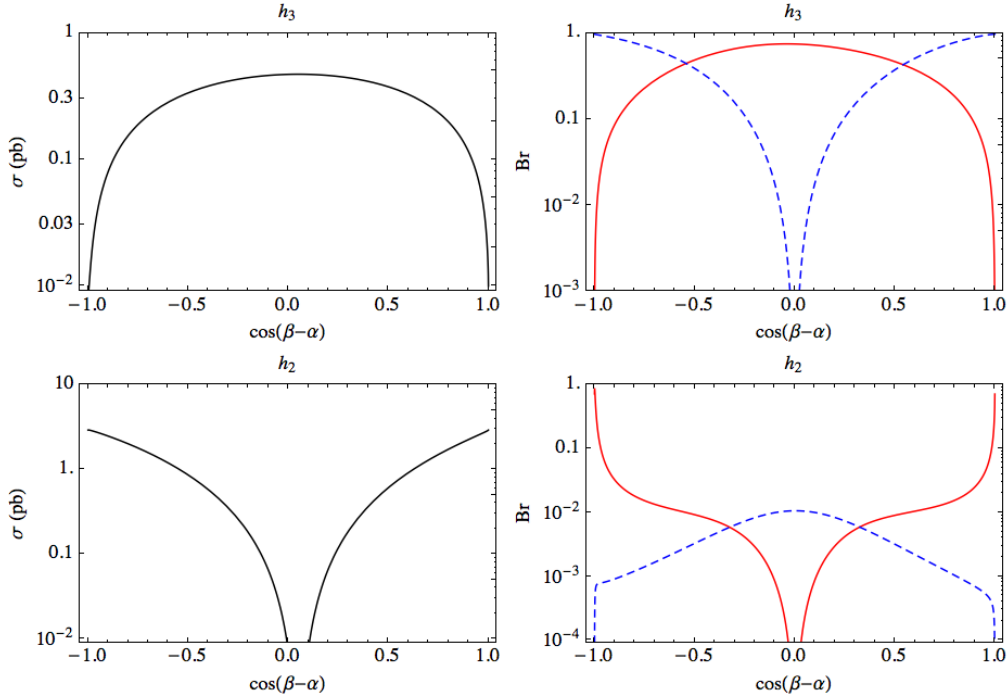


Figure 1. An example showing the impact of a non-zero CP violating angle, $\alpha_b = 0.5$, and the deviation from alignment (parameterized by $\cos(\beta - \alpha)$) on the heavy Higgs production from gluon fusion at $\sqrt{s} = 8$ TeV (left panels) and their decays (right panel) in $h_i \rightarrow VV$ (red, solid) and $h_i \rightarrow Zh_1$ (blue, dashed) channels. We have fixed the other parameters to be $\tan \beta = 20$, $\alpha_c = 0$, $m_{h_2} = 400$ GeV, $m_{h_3} = 450$ GeV and $\nu = 1$.

where g_{iz1} ($i = 2, 3$) is the coupling between h_i - Z - h_1 defined below Eq. (2.23). These make it manifest why the heavy Higgs to gauge boson decay channels are sensitive both to a deviation from the alignment limit and to CP violation. Clearly, when $\cos(\beta - \alpha) = \pm 1$, the decay rates $h_3 \rightarrow VV$ and $h_2 \rightarrow Zh_1$ vanish, while when $\cos(\beta - \alpha) = 0$, the decay rates $h_2 \rightarrow VV$ and $h_3 \rightarrow Zh_1$ vanish. For the case of h_2 decay, the branching ratios are more suppressed because the decay $h_2 \rightarrow h_1 h_1$ dominates in most of the parameter space. Therefore, the most important constraints come from the $h_3 \rightarrow VV$ and $h_3 \rightarrow Zh_1$ channels.

Combining Eqs. (2.28) and (2.29), we find the $h_3 \rightarrow VV$ signal rate (production cross section \times decay branching ratio) is peaked at $\cos(\beta - \alpha) = 0$, while $h_3 \rightarrow Zh_1$ vanishes at both $\cos(\beta - \alpha) = 0, \pm 1$, and is peaked in between. With these facts, one can understand the yellow and orange regions in the upper right panel of Fig. 11. One can also follow a similar analysis in order to understand the generic features in the other plots.

3 Results

In this section, we describe our method to obtain constraints from heavy Higgs searches at the LHC, and show the numerical results in a series of figures.

In the presence of CP violation, all of the three neutral scalars mix together, and we fix the lightest scalar, h_1 , to be the 126 GeV scalar already discovered at the LHC. As discussed in the previous sections, the heavy Higgs to gauge boson decay channels, including $h_{2,3} \rightarrow WW/ZZ$ and $h_{2,3} \rightarrow Zh_1 \rightarrow l^+l^-b\bar{b}$, are not only sensitive to deviations from the alignment limit ($\beta - \alpha = \pi/2$), but also to the presence of CP violation ($\alpha_b, \alpha_c \neq 0$). We use the production and decay rates calculated in Sec. 2.5 to obtain the 2HDM predictions for the heavy Higgs signal strength in these two channels. Then we compare these theory predictions to the results from the 7 and 8 TeV running of the LHC. For the heavy Higgs search data, we use limits for masses up to a TeV from the $h_{2,3} \rightarrow WW/ZZ$ channel [48, 49] and from the $h_{2,3} \rightarrow Zh_1 \rightarrow l^+l^-b\bar{b}(\tau^+\tau^-)$ channel [50, 51].

We also take into account the $h_{2,3} \rightarrow \tau^+\tau^-$ channel [52], which gives constraints for heavy Higgs masses up to a TeV and is relevant in the Type-II model in the large $\tan\beta$ case [53]. The experimental results are given as correlated fits to $\sigma(b\bar{b} \rightarrow h)BR(h \rightarrow \tau^+\tau^-)$ versus $\sigma(gg \rightarrow h)BR(h \rightarrow \tau^+\tau^-)$, which are shown in Fig. 8 of Ref. [52]. We interpret these bounds as bounds on the production of heavy Higgs states in the CP violating 2HDM. For the case $m_{h_2} = m_{h_3} = 300$ GeV, the limits are shown in Fig. 2³. In addition to a limit for $\tan\beta \gtrsim 30$, there is another limit around $\tan\beta \sim 1$. This lower limit arises because the masses of $h_{2,3}$ are below the $t\bar{t}$ threshold and hence the dominant decay channel is through $h_{2,3} \rightarrow b\bar{b}$ and $h_{2,3} \rightarrow \tau^+\tau^-$. For $m_{h_2} = m_{h_3} = 500$ GeV the bound from $h_{2,3} \rightarrow \tau^+\tau^-$ gives no constraint for $\tan\beta < 50$. In general, we find that the bounds from $h_{2,3} \rightarrow \tau^+\tau^-$ are always weaker than those from the coupling measurement of the light Higgs or EDMs. As a result, we will not include them in the following plots.

The most up-to-date 126 GeV Higgs coupling data are given in Table 2, normalized to the appropriate luminosities. They are used to constrain the theoretical predictions for the signal rates of h_1 , from Sec. 2.5. We take the SM cross sections from the LHC Higgs Cross Section Working Group [43]. We have performed a χ^2 analysis using the results listed in Table 2.

In Figs. 3 to 12, we show the limits derived from heavy Higgs searches and the light (126 GeV) Higgs data, together with those from the low energy electron and neutron EDMs. For the EDM constraints, we use the results of Ref. [10].

In these numerical results, we fix the heavy Higgs masses and the parameter $\nu = 1$. The CP violating angle α_c is fixed in the approximate Z_2 symmetric model by Eq. (2.12). On the other hand, for the extended model without an approximate Z_2 symmetry, α_c is a free parameter. We also note that varying the parameter ν between 0 and 1 only leads to slight changes to our results. The constraints are shown in the $\sin\alpha_b$ versus $\tan\beta$ plane, while varying α and α_c . We consider both the alignment limit with $\alpha = \beta - \pi/2$ and cases when

³We assume that there is no interference between the h_2 and h_3 resonances.

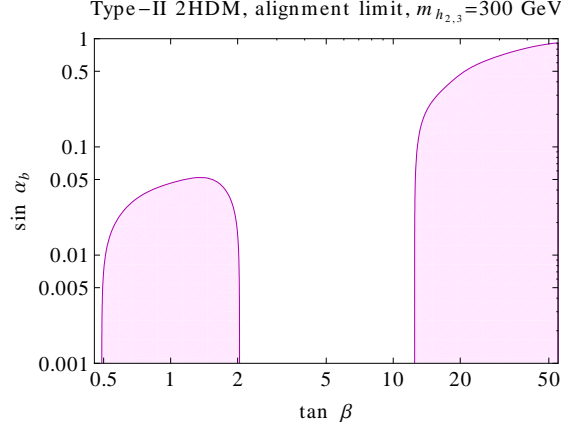


Figure 2. Heavy Higgs search constraints on the Type-II 2HDM with approximate Z_2 symmetry and $m_{h_2} = m_{h_3} = 300$ GeV. The colored regions are excluded by the search for $h_{2,3} \rightarrow \tau^+ \tau^-$.

Table 2. ATLAS and CMS Higgs Coupling Measurements.

Channel	μ_{CMS}	Ref.	μ_{ATLAS}	Ref.
μ_{WW}	0.83 ± 0.21	[54]	$1.09^{+0.23}_{-0.21}$	[55]
μ_{ZZ}	1.0 ± 0.29	[54]	$1.44^{+0.40}_{-0.33}$	[56]
$\mu_{\gamma\gamma}$	1.13 ± 0.24	[54]	1.17 ± 0.27	[57]
μ_{bb}	0.93 ± 0.49	[54]	0.5 ± 0.4	[58]
$\mu_{\tau\tau}$	0.91 ± 0.27	[54]	1.4 ± 0.4	[59]

there are small deviations from alignment, $\cos(\beta - \alpha) = \pm\Delta$. The 126 GeV Higgs data put upper bounds on Δ for fixed values of $\tan\beta$. For the Type-I model, we consider $\Delta = 0.1$, while for the Type-II model, the light Higgs coupling data constraint is stronger at large $\tan\beta$, so we take $\Delta = 0.02$ [4]. ATLAS has also limited the parameters of the 2HDM by directly searching for the heavier neutral Higgs boson, but these limits are not competitive with the Higgs coupling data for the heavy $h_{2,3}$ masses that we consider [47].

3.1 Limits from Heavy Higgs Searches in Approximate Z_2 Symmetric Models

We first discuss the models with an approximate Z_2 symmetry. Fig. 3 shows the limits on the CP violating parameter, α_b , as a function of $\tan\beta$ in the Type-I model. In each panel, the gray area marked “theory inaccessible” has no real solution for α_c from Eq. (2.12). The left panel assumes the alignment limit, $\beta - \alpha \sim \pi/2$, while the right panel allows for a small deviation from the alignment limit⁴. The orange area is excluded by the heavy Higgs search channel $h_{2,3} \rightarrow Zh_1 \rightarrow l^+ l^- b\bar{b}$, while the yellow area is excluded by the channel $h_{2,3} \rightarrow WW/ZZ$. It is clear that the limits become quite stringent away from the alignment limit. For comparison,

⁴The results are similar for negative Δ .

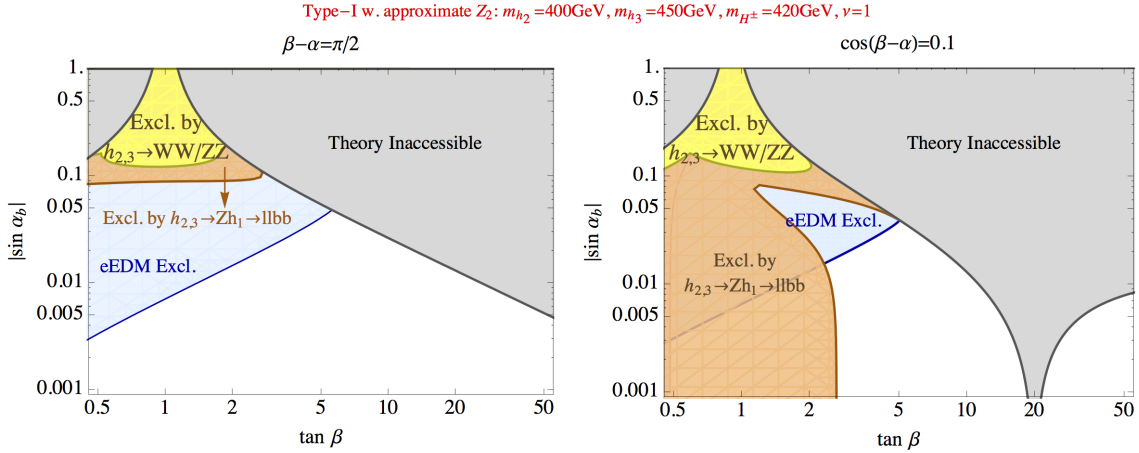


Figure 3. Heavy Higgs search constraints on the Type-I 2HDM with approximate Z_2 symmetry, using the $h_{2,3} \rightarrow WW/ZZ$ (yellow) and $h_{2,3} \rightarrow Zh_1 \rightarrow l^+l^-b\bar{b}$ (orange) channels. These constraints are presented in the $\sin \alpha_b$ versus $\tan \beta$ parameter space and colored regions are excluded. The left panel is for the alignment limit with $\alpha = \beta - \pi/2$, while the right panel shows the case with a deviation from that limit. Also shown in blue are the electron EDM excluded regions. In these plots, we have chosen the heavy scalar masses to be $m_{h_2} = 400$ GeV, $m_{h_3} = 450$ GeV, $m_{H^\pm} = 420$ GeV, and the model parameter $\nu = 1$. The other mixing angle α_c is a dependent quantity fixed by Eq. (2.12). In the gray region, there is no real solution for α_c .

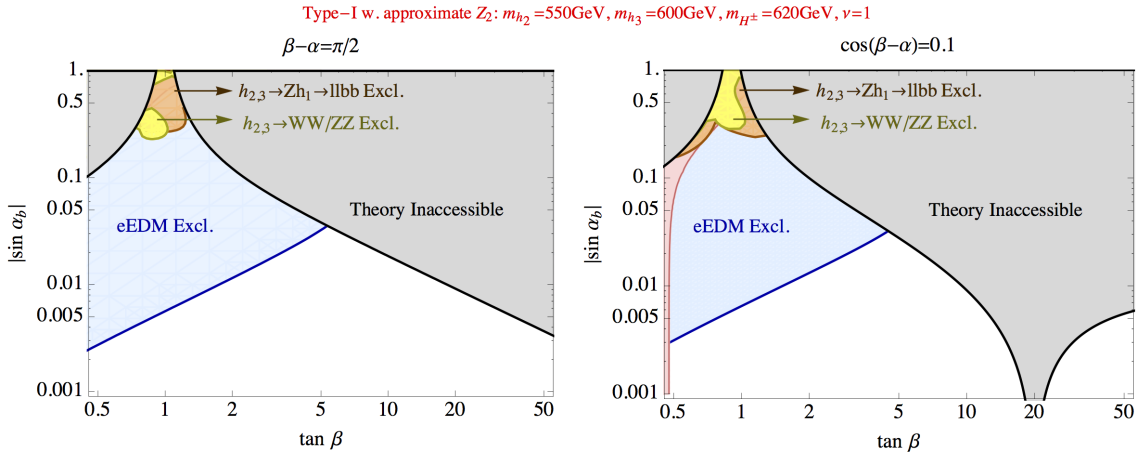


Figure 4. Similar to Fig. 3, but with heavy scalar masses $m_{h_2} = 550$ GeV, $m_{h_3} = 600$ GeV, $m_{H^\pm} = 620$ GeV. In the right panel, the red region is excluded by the 126 GeV Higgs data applied to h_1 .

we include the results of Ref. [10] for the limits from the electron EDM (eEDM, the blue shaded regions are excluded). In all cases, the EDM limit and the heavy Higgs searches exclude complementary regions. The masses of the heavy Higgs are increased to around 600 GeV in Fig. 4. In this case, the limits from heavy Higgs searches become much weaker, with

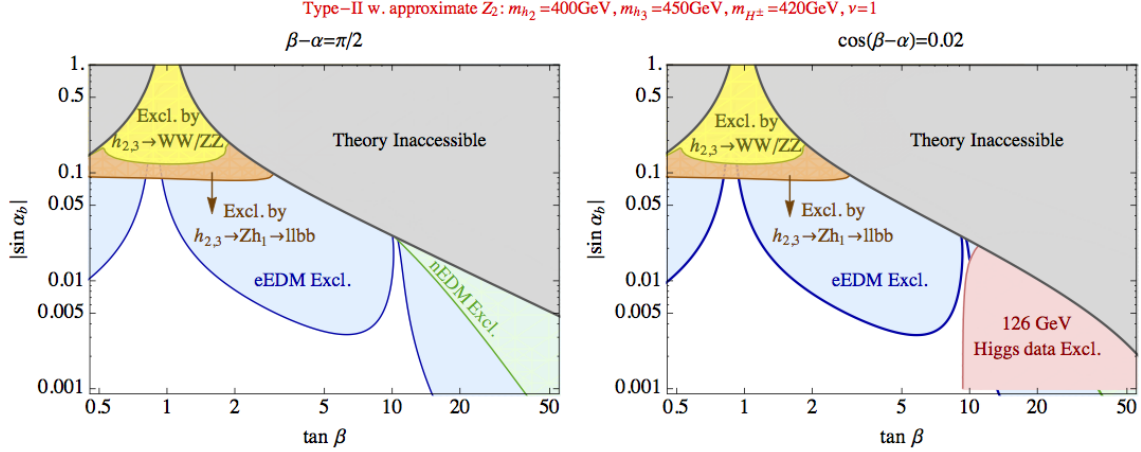


Figure 5. Heavy Higgs search constraints on the Type-II 2HDM with approximate Z_2 symmetry. The Higgs sector parameters are chosen to be the same as those in Fig. 3. The colored regions are excluded by searches for $h_{2,3} \rightarrow WW/ZZ$ (yellow), $h_{2,3} \rightarrow Zh_1 \rightarrow l^+l^-b\bar{b}$ (orange) channels, 126 GeV Higgs coupling data (red), electron EDM measurements (blue), and neutron EDM limits (green). The gray region is again theoretically excluded because it contains no real solution for α_c .

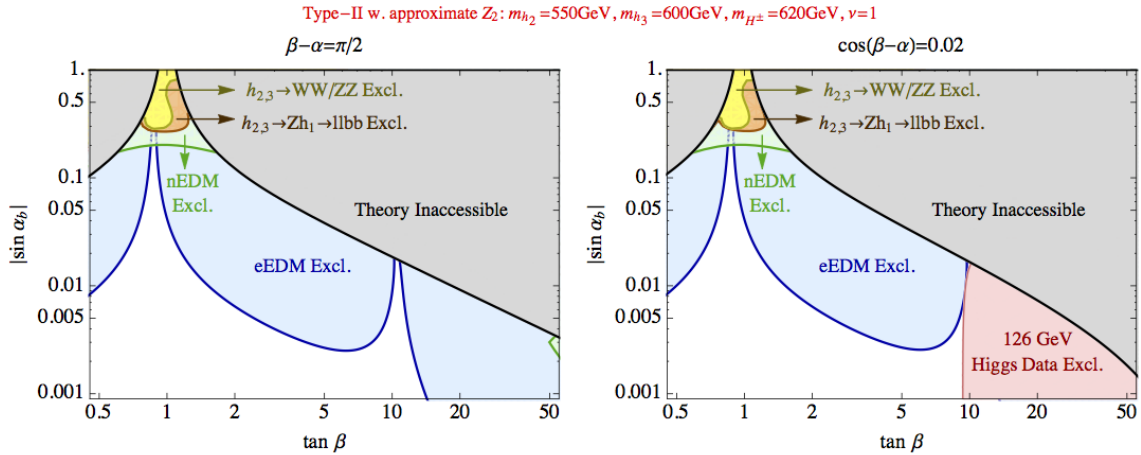


Figure 6. Similar to Fig. 5, but with heavy scalar masses $m_{h_2} = 550$ GeV, $m_{h_3} = 600$ GeV, $m_{H^\pm} = 620$ GeV.

the dominant excluded region coming from the eEDM searches. The mass splitting between the heavy masses is restricted by limits on the oblique parameters, which is discussed in Sec. 4.1.

Fig. 5 shows the limits on α_b versus $\tan \beta$ in the Type-II model. Away from the alignment limit (the right panel), there is a significant exclusion region for $\tan \beta \gtrsim 10$ from the 126 GeV Higgs parameter measurements. Around $\tan \beta \sim 1$, the electron EDM constraint vanishes due to a cancellation among the Barr-Zee diagrams as pointed out in Ref. [8]. We find the heavy Higgs searches from the gauge boson decay channels $h_{2,3} \rightarrow Zh_1$ and $h_{2,3} \rightarrow WW/ZZ$

are extremely useful and close the window of large values of $\sin \alpha_b \sim \mathcal{O}(1)$ in all cases. As the mass of the heavy particles is increased in Fig. 6, the region excluded by the heavy Higgs searches shrinks, with again the dominant exclusion coming from the eEDM and neutron EDM (nEDM, the green regions are excluded). It is worth pointing out that the neutron EDM excluded regions are shown using the central values given in [60], which however involves large uncertainties in the evaluation of hadronic matrix elements. In contrast, the heavy Higgs searches provide a robust upper limit on the CP violating angle α_b .

3.2 Limits from Heavy Higgs Searches in the Models with no Z_2 Symmetry

As discussed in Sec. 2.4, if the assumption of an approximate Z_2 symmetry is relaxed, the theoretical relationship between α_b and α_c can be removed. In this case α_c becomes a free parameter. This helps to remove the theoretically inaccessible region in Figs. 3–6, and one can get a complete view of various constraints in the whole parameter space.

Figs. 7 and 8 show the constraints in the Type-I model with α_c chosen equal to 0 or α_b , and with two sets of heavy Higgs masses. It is apparent that the dependence on α_c is rather weak. The results in the Type-II model are shown in Figs. 9 and 10. In Figs. 11 and 12, the heavy Higgs search constraints are also displayed in the α_b and $\cos(\beta - \alpha)$ plane.

It is also worth re-emphasizing that at low $\tan \beta \sim \mathcal{O}(1)$ the 126 GeV Higgs data puts a very weak constraint on the CP violating angle α_b . This can also be understood from Table 1, where the lightest (126 GeV) Higgs couplings to other SM particles near the alignment limit are

$$\begin{aligned}
a_1 &\simeq \cos \alpha_b, & c_{t,1} &\simeq (1 + \Delta \cot \beta) \cos \alpha_b, & \tilde{c}_{t,1} &\simeq -\cot \beta \sin \alpha_b, \\
c_{b,1} &\simeq \begin{cases} (1 + \Delta \cot \beta) \cos \alpha_b, & \text{Type - I} \\ (1 - \Delta \tan \beta) \cos \alpha_b, & \text{Type - II} \end{cases} & \tilde{c}_{b,1} &\simeq \begin{cases} \cot \beta \sin \alpha_b, & \text{Type - I} \\ -\tan \beta \sin \alpha_b, & \text{Type - II} \end{cases} \quad (3.1)
\end{aligned}$$

where $\Delta = \cos(\beta - \alpha)$ and we have kept terms up to first power in Δ . Clearly for small Δ and $\tan \beta \approx 1$, all CP even couplings are approximately $\cos \alpha_b$ and all CP odd couplings $\approx \pm \sin \alpha_b$. They approach the values in the SM limit when $\alpha_b \rightarrow 0$. In the presence of CP violation, the gluon fusion production cross section of the light Higgs gets rescaled from the SM value by a factor [8, 10], $\sigma(gg \rightarrow h_1)/\sigma_{\text{SM}}(gg \rightarrow H_{SM}) \simeq 1 + 1.42 \sin^2 \alpha_b$. The vector boson fusion and associated production rates get suppressed by $\sigma(VV \rightarrow h_1)/\sigma_{\text{SM}}(VV \rightarrow H_{SM}) = \cos^2 \alpha_b$. The light Higgs to fermion ($h_1 \rightarrow b\bar{b}, \tau^+\tau^-$) decay rates are not affected because the CP even and CP odd couplings contribute incoherently, $\Gamma(h_1 \rightarrow f\bar{f})/\Gamma_{\text{SM}}(h \rightarrow f\bar{f}) = \cos^2 \alpha_b + \sin^2 \alpha_b = 1$. The Higgs to gauge boson ($h_1 \rightarrow WW^*, ZZ^*$) decay rates get suppressed, $\Gamma(h_1 \rightarrow VV^*)/\Gamma_{\text{SM}}(h_1 \rightarrow VV^*) = \cos^2 \alpha_b$. The light Higgs to diphoton decay rate in the presence of CP violation has been given in refs. [8, 10], which in this case can be simplified to $\Gamma(h_1 \rightarrow \gamma\gamma)/\Gamma_{\text{SM}}(h \rightarrow \gamma\gamma) \simeq 1 - 0.81 \sin^2 \alpha_b$. As a result, the final χ^2 of the fit for the 126 GeV Higgs data depends on $\cos^2 \alpha_b$, and for the SM case $\chi_{\text{SM}}^2 = \chi^2(\cos^2 \alpha_b \rightarrow 1)$. Because the $\cos^2 \alpha_b$ function is very flat near $\alpha_b = 0$, one can maintain a fit as good as in the SM for sizable α_b .

In contrast, the heavy Higgs decay to gauge boson channels ($h_{2,3} \rightarrow VV$ and Zh_1) are more sensitive to a non-zero CP violating angle α_b and can place a stronger constraint on it. This feature has been discussed in Sec. 2.6. Furthermore, from the figures we notice that at low $\tan\beta$, the heavy Higgs search constraint is stronger than at large $\tan\beta$. This is because $h_i \rightarrow t\bar{t}$, ($i = 2, 3$) is the dominant decay mode and the branching ratio for the gauge boson decay modes of h_i can be written as

$$\text{Br}_{h_i \rightarrow VV \text{ or } Zh}(\text{low } \tan\beta) \sim \frac{\Gamma_{h_i \rightarrow VV \text{ or } Zh}}{\Gamma_{h_i \rightarrow t\bar{t}}} . \quad (3.2)$$

Eqs. (2.28) and (2.29) tell us that these two rates around the alignment limit are both insensitive to variations of $\tan\beta$. However, as $\tan\beta$ grows to larger than $\mathcal{O}(2)$, the other decay channels such as $h_i \rightarrow h_1 h_2$ and $h_i \rightarrow b\bar{b}$ larger than $h_i \rightarrow t\bar{t}$, and they are not yet constrained by the LHC data. As a result, the gauge boson decay rates of heavy Higgs bosons are suppressed in this region.

Fig. 13 depicts 95% CL constraints in the $\tan\beta$ versus $\cos(\beta - \alpha)$ plane from heavy Higgs searches (black) and from 126 GeV Higgs data (yellow) on the Type-I (first row) and Type-II (second row) 2HDMs without approximate Z_2 symmetry. Different curves correspond to $\alpha_b = 0$ (dotted), 0.1 (solid) and 0.5 (dashed), and the other mixing angle $\alpha_c = 0$. For the CP conserving case ($\alpha_b = 0$), we found that the bounds are very similar to those studied in Refs. [5, 34, 35, 61]. In both Type-I and Type-II models, both heavy and light Higgs searches favor regions around the alignment limit $\cos(\beta - \alpha) = 0$. In the Type-II model when CP violation is small (bottom left panel), there is another allowed branch corresponding to $\cos(\beta + \alpha) \sim 0$ [62], but we find the heavy and light Higgs favored regions are inconsistent with each other for very large deviations from the alignment limit. In the Type-I model (first row), the light Higgs bound only depends on $\cos(\beta - \alpha)$, but is independent of $\tan\beta$ in the large $\tan\beta$ limit. The reason is that in this case the h_1 couplings can be approximated as $c_{t,1} = c_{b,1} \rightarrow \sin(\beta - \alpha) \cos\alpha_b + \mathcal{O}(1/\tan\beta)$, $\tilde{c}_{t,1} = -\tilde{c}_{b,1} = \mathcal{O}(1/\tan\beta)$ and $a_1 = \sin(\beta - \alpha) \cos\alpha_b$, so their dependence on $\tan\beta$ is suppressed. On the other hand, for the Type-II model, the couplings $c_{b,1}$, $c_{\tau,1}$ and $\tilde{c}_{b,1}$, $\tilde{c}_{\tau,1}$ are enhanced at large $\tan\beta$. This explains why in the Type-II model (second row), light Higgs data are more restrictive on the parameter space with large $\tan\beta$. As a result, for $\alpha_b = 0.5$, the light Higgs data only favors a region with $\tan\beta \lesssim 2$ (see the bottom right panel of Fig. 13). In contrast, we have learned that the heavy Higgs search data are more sensitive at small $\tan\beta$ and for $\alpha_b = 0.5$ they only allow the region where $\tan\beta \gtrsim 3$, thus there is no region in the parameter space that can be made consistent with both light and heavy Higgs results from LHC. Fig. 14 gives results similar to those in Fig. 13 but with a different set of mass parameters, $m_{h_2} = 550$ GeV, $m_{h_3} = 600$ GeV, $m_{H^+} = 620$ GeV. The parameter space becomes less constrained by the heavy Higgs searches because the production cross sections are smaller compared to those in Fig. 13.

From the above results, we can conclude that if the heavy Higgs masses lie below around 600 GeV, the CP violating phase α_b is constrained to be less than around 30% throughout the most general parameter space. The regions which allow α_b close to this upper bound are

$\tan \beta \sim 1$ in the Type-II model, and $\tan \beta \gtrsim 20$ in the Type-I model without an approximate Z_2 symmetry. We have also estimated the future sensitivity of the heavy Higgs search at the 14 TeV LHC by rescaling the current limits by the square root of expected number of events ($\sigma \times \mathcal{L}$). With 300 (3000) fb^{-1} data, if the heavy Higgs masses are below 600 GeV and we still do not find them, the CP violating angle α_b will be constrained to be less than around 10%.

Recall that the angle α_b parametrizes the size of CP odd mixture in the 126 GeV Higgs boson. The main point of this work is to show that the heavy Higgs search is relevant and plays a complimentary role to the other indirect searches, and sometimes it stands at the frontier of probing the Higgs boson CP mixture.

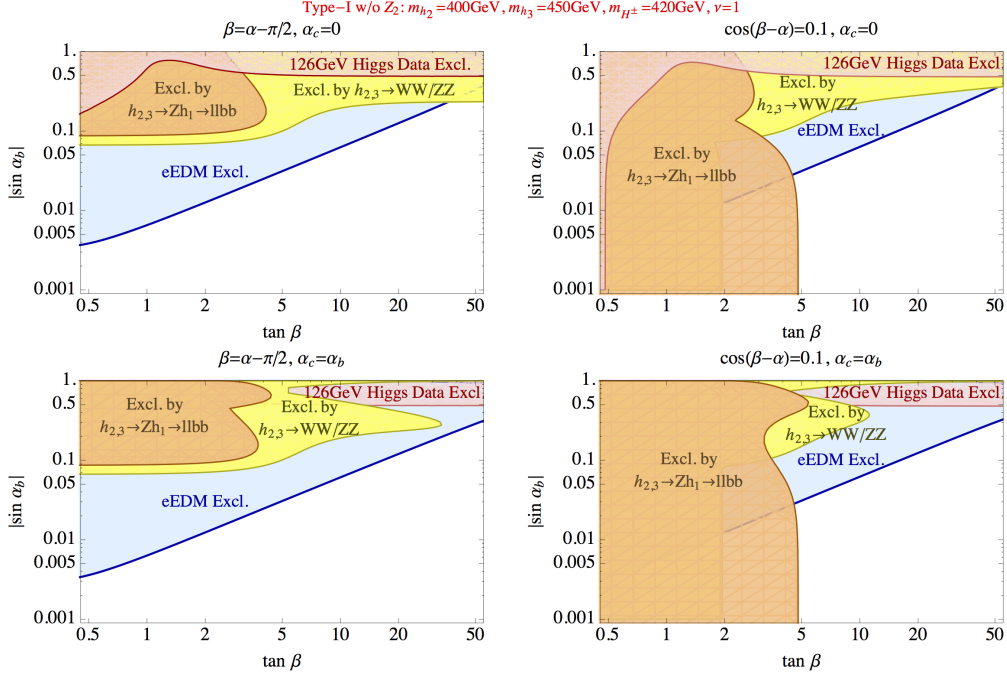


Figure 7. Heavy Higgs search constraints on the Type-I 2HDM without approximate Z_2 symmetry, *i.e.*, in this case α_c is a free parameter which is allowed to vary. The color scheme for the exclusion regions is the same as in Figs. 3–6. The first two rows use the same parameters as Fig. 3, and the last two rows use the same as Fig. 4.

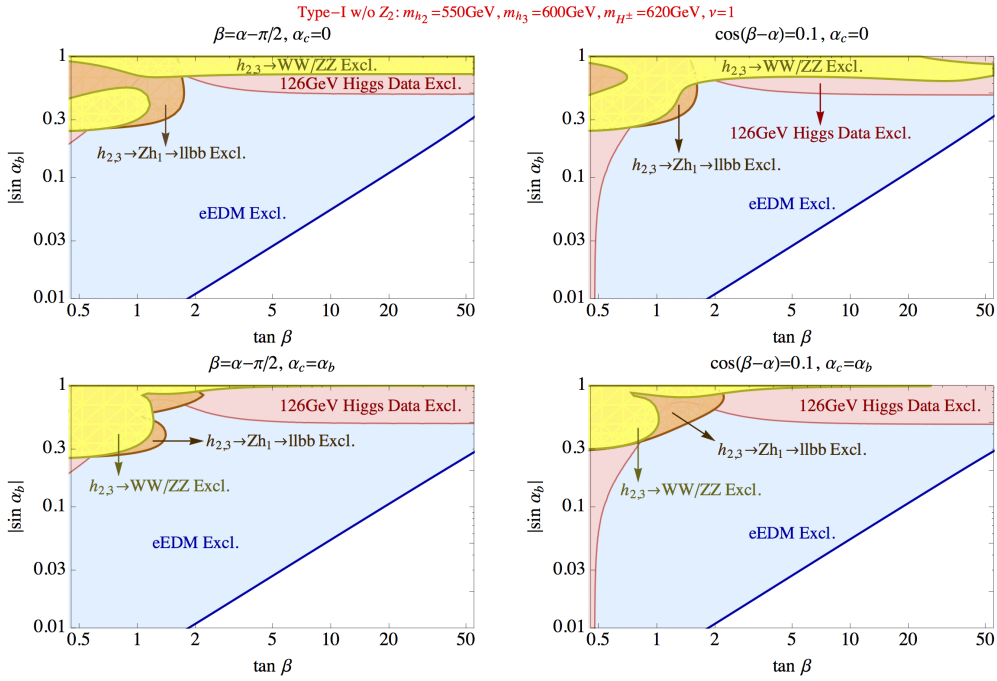


Figure 8. Similar to Fig. 7, but with heavy Higgs masses $m_{h_2} = 550\text{ GeV}$, $m_{h_3} = 600\text{ GeV}$, $m_{H^\pm} = 620\text{ GeV}$.

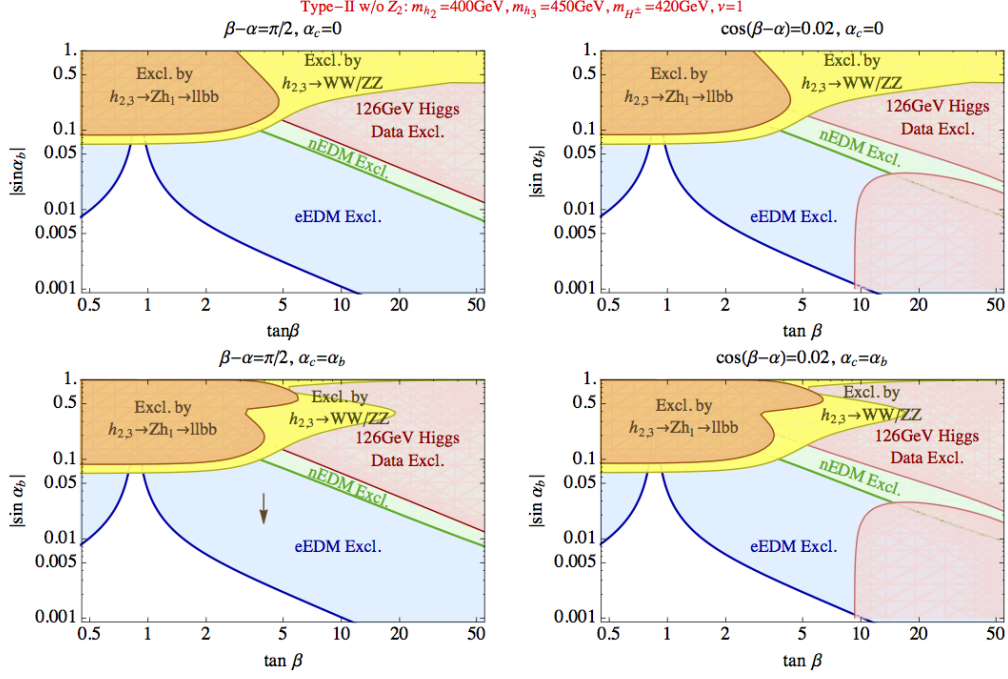


Figure 9. Similar to Fig. 7, but for the Type-II 2HDM without approximate Z_2 symmetry.

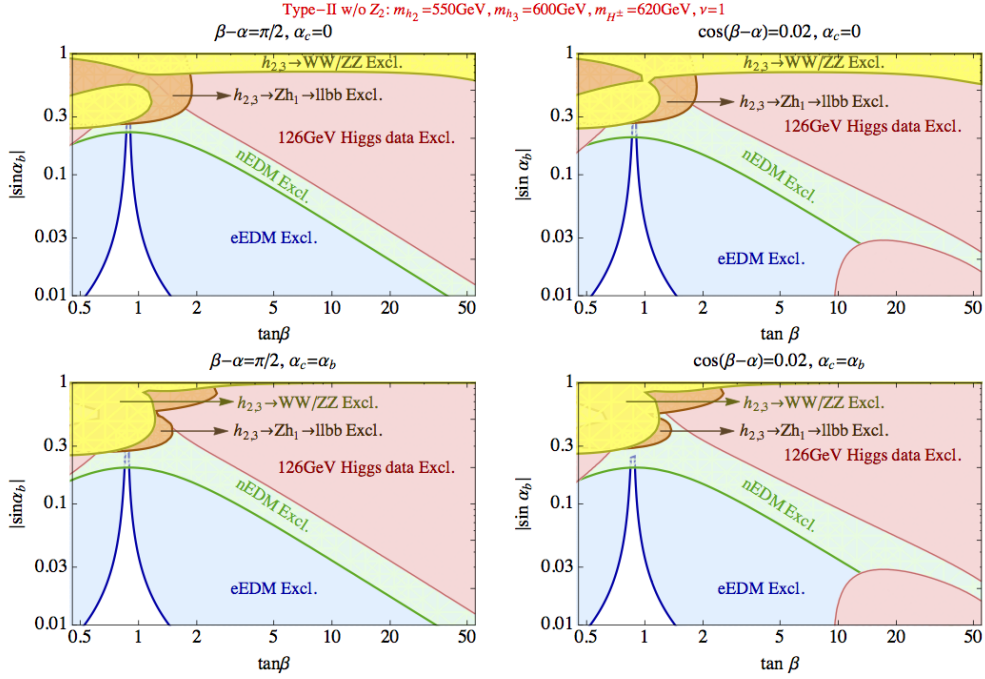


Figure 10. Similar to Fig. 8, but for the Type-II 2HDM without approximate Z_2 symmetry.

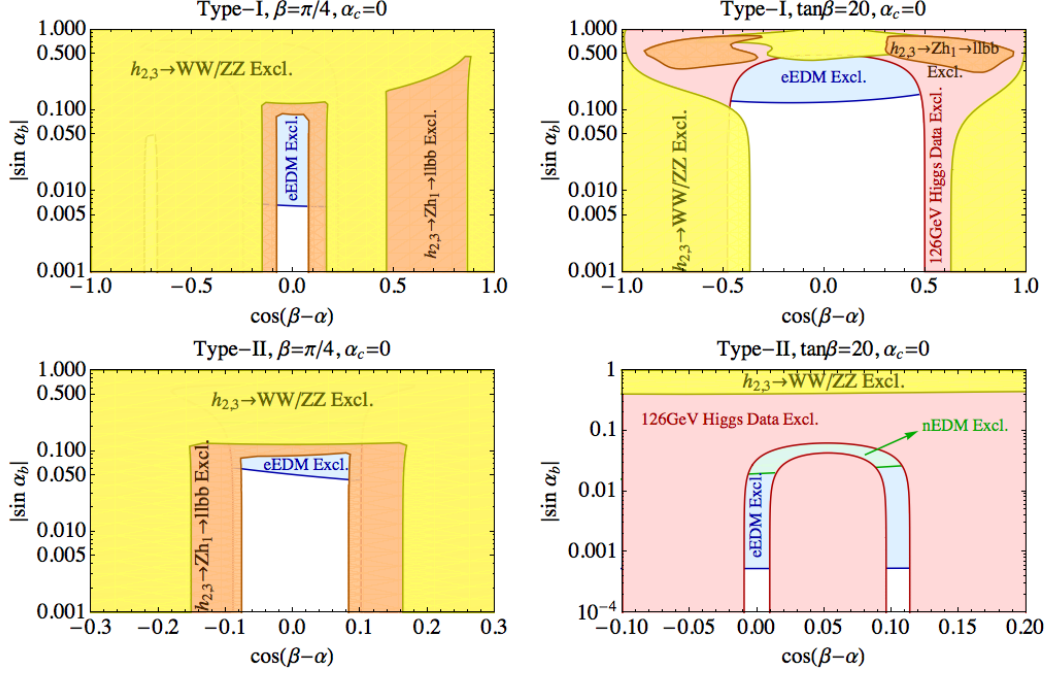


Figure 11. Heavy Higgs search constraints on the Type-I (first row) and Type-II (second row) 2HDM without approximate Z_2 symmetry, using the $h_{2,3} \rightarrow WW/ZZ$ (yellow) and $h_{2,3} \rightarrow Zh_1 \rightarrow l^+l^-b\bar{b}$ (orange) channels. The heavy scalar masses are fixed to be $m_{h_2} = 400$ GeV, $m_{h_3} = 450$ GeV, $m_{H^+} = 420$ GeV, and the model parameter $\nu = 1$. The other mixing angle $\alpha_c = 0$.

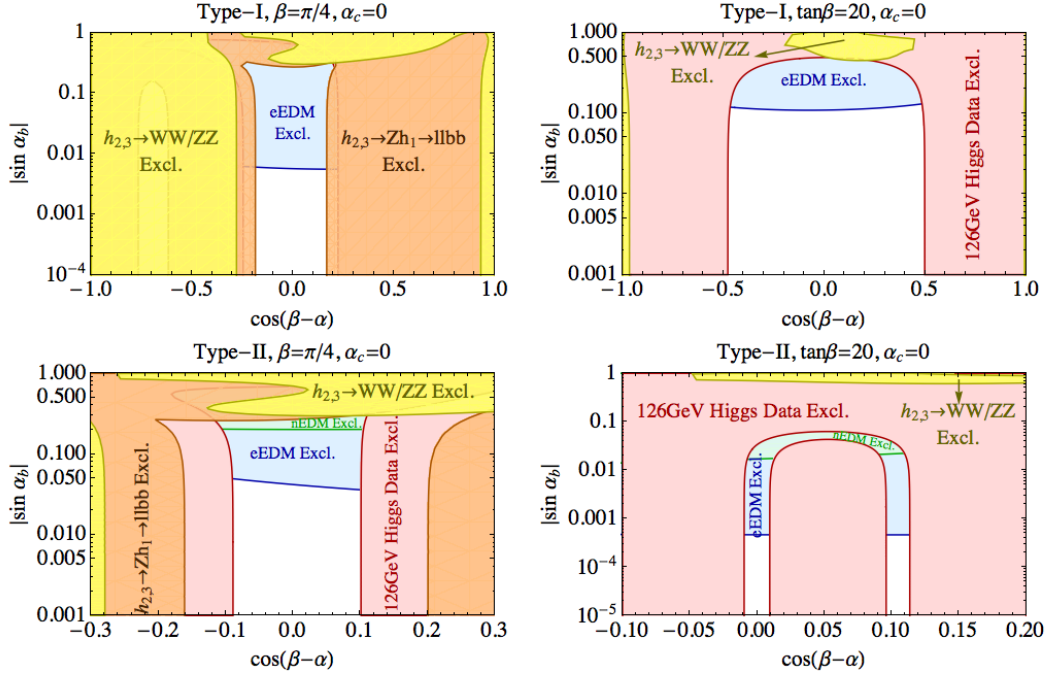


Figure 12. Similar to Fig. 11, but with heavy scalar masses $m_{h_2} = 550$ GeV, $m_{h_3} = 600$ GeV, $m_{H^+} = 620$ GeV.

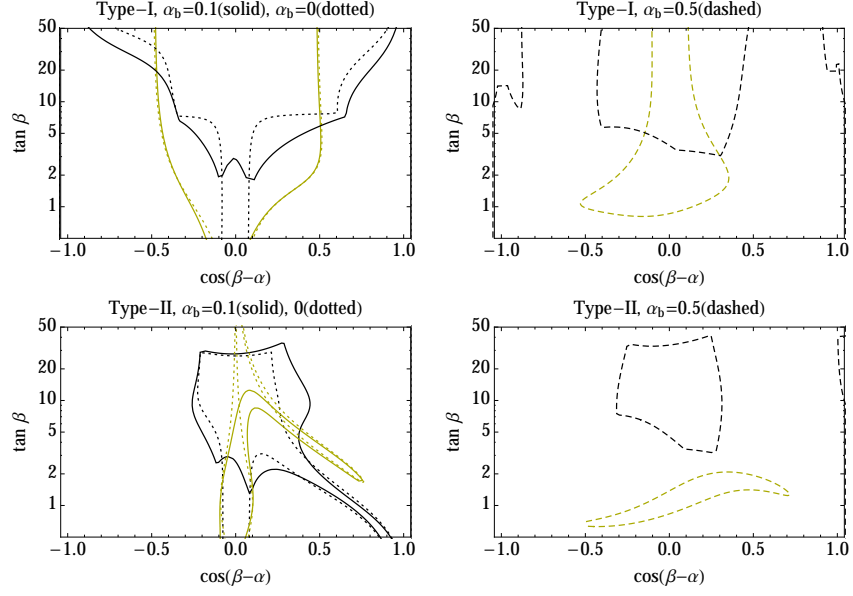


Figure 13. Heavy Higgs search (black) and 126 GeV Higgs data (yellow) constraints at 95% CL on the Type-I (first row) and Type-II (second row) 2HDM without approximate Z_2 symmetry. Different curves correspond to $\alpha_b = 0$ (dotted), 0.1 (solid) and 0.5 (dashed). The heavy Higgs curves include the combination of constraints from $h_{2,3} \rightarrow WW/ZZ$, $h_{2,3} \rightarrow Zh_1 \rightarrow l^+l^-b\bar{b}$ and $h_{2,3} \rightarrow \tau^+\tau^-$ channels. The heavy scalar masses are fixed to be $m_{h_2} = 400$ GeV, $m_{h_3} = 450$ GeV, $m_{H^\pm} = 420$ GeV, and the model parameter $\nu = 1$. The other mixing angle $\alpha_c = 0$.

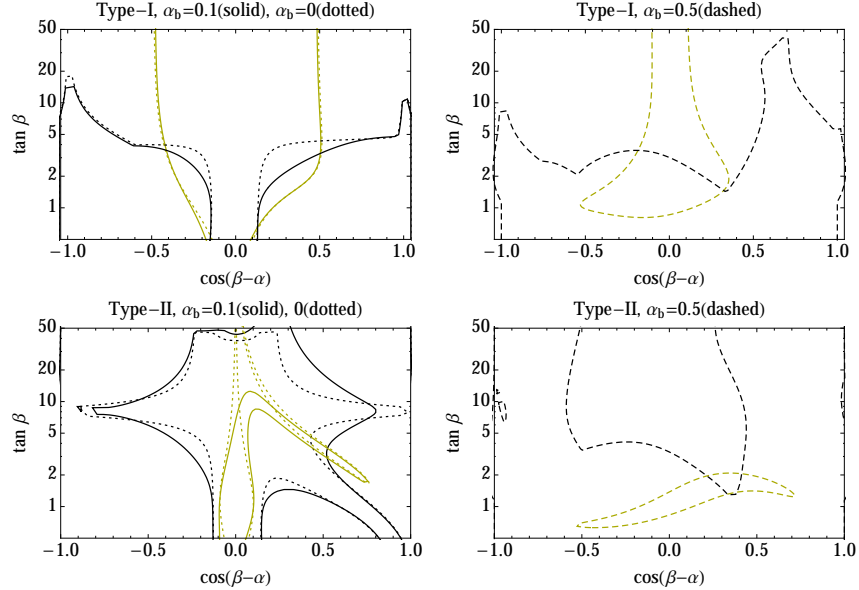


Figure 14. Similar to Fig. 13, but for heavy Higgs masses $m_{h_2} = 550$ GeV, $m_{h_3} = 600$ GeV, $m_{H^\pm} = 620$ GeV.

4 Limits from B Decays, Oblique Parameters, and $(g-2)_\mu$

The CP violating 2HDM is also limited by measurements in B decays, the oblique parameters, and $(g-2)_\mu$. In Type-II models the charged Higgs mass is restricted by B data to be greater than $m_{H^+} \sim 340$ GeV for all values of $\tan\beta$. In both Type-1 and Type-2 models, measurements in the B system prefer $\tan\beta > 1$ [5, 63, 64].

4.1 Limits from Electroweak Oblique Parameters

The allowed parameters are restricted by measurements of the oblique parameters. The general results for S, T and U in a 2HDM are given in Refs. [3, 65–67]. In the alignment limit, $\cos\alpha = \sin\beta$ and $\sin\alpha = -\cos\beta$, the results simplify considerably,

$$\begin{aligned} \alpha\Delta T = \frac{1}{16\pi^2 v^2} & \left\{ \sin^2\alpha_b F(m_{H^+}^2, m_{h_1}^2) + (1 - \sin^2\alpha_b \sin^2\alpha_c) F(m_{H^+}^2, m_{h_2}^2) \right. \\ & + (1 - \sin^2\alpha_b \cos^2\alpha_c) F(m_{H^+}^2, m_{h_3}^2) - \cos^2\alpha_c \sin^2\alpha_b F(m_{h_1}^2, m_{h_2}^2) \\ & - \sin^2\alpha_c \sin^2\alpha_b F(m_{h_1}^2, m_{h_3}^2) - \cos^2\alpha_b F(m_{h_2}^2, m_{h_3}^2) \\ & + 3 \cos^2\alpha_b \left[F(M_Z^2, m_{h_1}^2) - F(M_W^2, m_{h_1}^2) \right] \\ & + 3 \sin^2\alpha_c \sin^2\alpha_b \left[F(M_Z^2, m_{h_2}^2) - F(M_W^2, m_{h_2}^2) \right] \\ & + 3 \cos^2\alpha_c \sin^2\alpha_b \left[F(M_Z^2, m_{h_3}^2) - F(M_W^2, m_{h_3}^2) \right] \\ & \left. - 3 \left[F(M_Z^2, M_{H,ref}^2) - F(M_W^2, M_{H,ref}^2) \right] \right\}, \end{aligned} \quad (4.1)$$

where the last line is the subtraction of the SM Higgs contribution evaluated at the reference scale, $M_{H,ref}$, at which the fit to the data is performed. The function $F(x, y)$ is,

$$\begin{aligned} F(x, y) &= \frac{x+y}{2} - \frac{xy}{(x-y)} \log\left(\frac{x}{y}\right). \\ F(x, x) &= 0, \\ F(x, y) &\xrightarrow{y \gg x} \frac{y}{2}. \end{aligned} \quad (4.2)$$

With $\alpha_c=0$, we obtain the simple form,

$$\alpha\Delta T = \frac{1}{12\pi^2 v^2} \left\{ \Delta_2 \Delta_3 \cos^2\alpha_b + \left[\Delta_1 \Delta_2 - 2(\Delta_3 - \Delta_1)(M_W - M_Z) \right] \sin^2\alpha_b \right\} \quad (4.3)$$

and $\Delta_i \equiv m_{H^+} - m_{h_i}$. Eq. (4.3) is in agreement with Ref. [68] in the limit $\alpha_b = 0$.

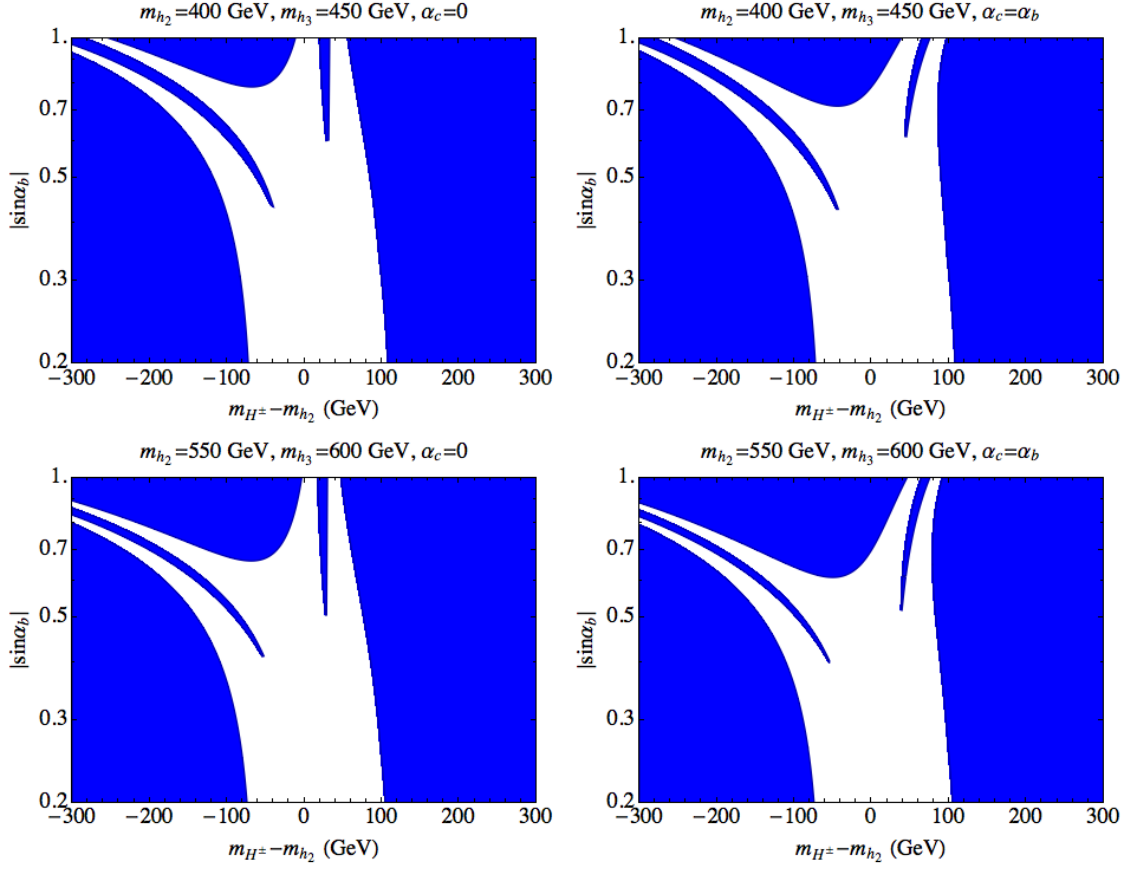


Figure 15. 95% Confidence Level allowed regions (white) from fits to the oblique parameters in the CP violating 2HDM.

The result for ΔS also takes a simple form in the alignment limit [65],

$$\begin{aligned}
\Delta S = \frac{1}{24\pi} & \left\{ \cos^2 2\theta_W G(m_{H^+}^2, m_{H^+}^2, M_Z^2) + \sin^2 \alpha_b \left[\cos^2 \alpha_c G(m_{h_1}^2, m_{h_2}^2, M_Z^2) \right. \right. \\
& \left. \left. + \sin^2 \alpha_c G(m_{h_1}^2, m_{h_3}^2, M_Z^2) + \sin^2 \alpha_c \hat{G}(m_{h_2}^2, M_Z^2) + \cos^2 \alpha_c \hat{G}(m_{h_3}^2, M_Z^2) \right] \right. \\
& \left. + \cos^2 \alpha_b \left[\hat{G}(m_{h_1}^2, M_Z^2) + G(m_{h_2}^2, m_{h_3}^2, M_Z^2) \right] + \ln \left(\frac{m_{h_1}^2 m_{h_2}^2 m_{h_3}^2}{m_{H^+}^6} \right) \right. \\
& \left. - \left[\hat{G}(M_{H,ref}^2, M_Z^2) + \ln \left(\frac{M_{H,ref}^2}{m_{H^+}^2} \right) \right] \right\}. \tag{4.4}
\end{aligned}$$

Analytic results for $G(x, y, z)$ and $\hat{G}(x, y)$ are given in the appendix of Ref. [65].

We use the Gfitter fit to the electroweak data [69],

$$\begin{aligned} S &= 0.05 \pm 0.11 \\ T &= 0.09 \pm 0.13 \\ U &= 0.01 \pm 0.11, \end{aligned} \tag{4.5}$$

with a reference value for the SM Higgs mass, $M_{H,ref} = 125 \text{ GeV}$. The STU correlation matrix is,

$$\rho_{ij} = \begin{pmatrix} 1 & 0.90 & -0.59 \\ 0.09 & 1 & -0.83 \\ -0.59 & -0.83 & 1 \end{pmatrix}, \tag{4.6}$$

and the χ^2 is defined as

$$\Delta\chi^2 = \Sigma_{ij}(\Delta X_i - \Delta\hat{X}_i)(\sigma^2)_{ij}^{-1}(\Delta X_j - \Delta\hat{X}_j), \tag{4.7}$$

where $\hat{X}_i = \Delta S, \Delta T$, and ΔU are the central values of the fit in Eq. (4.5), $\hat{X}_i = \Delta S, \Delta T$, and ΔU are the parameters in the 2HDM (Eqs. (4.1) and (4.4)), σ_i are the errors given in Eq. (4.5) and $\sigma_{ij}^2 = \sigma_i \rho_{ij} \sigma_j$.

In Fig. 15 we show the 95% confidence level allowed regions for $\alpha_b = \alpha_c$ and $\alpha_c = 0$. For α_b close to 1, there is some interesting structure due to the interplay of the ΔS and ΔT limits. For $|\sin \alpha_b| < 0.5$, the results are well approximated by the limit from ΔT only,

$$-80 \text{ GeV} < \Delta_2 < 120 \text{ GeV}. \tag{4.8}$$

4.2 Limits from muon $g - 2$

The experimentally measured value of $\frac{(g-2)_\mu}{2} = a_\mu$ places a weak constraint on the parameters of the CP violating 2HDM. The deviation between the experimental number and the SM theory prediction is [70],

$$\Delta a_\mu = a_\mu^{exp} - a_\mu^{SM} = 265(85) \times 10^{-11}. \tag{4.9}$$

The one-loop contributions from the Higgs sector in the 2HDM to Δa_μ are numerically small. The larger Higgs sector contributions come from the 2-loop Barr-Zee type diagrams with a closed fermion/gauge-boson/heavy-Higgs loop. This class of diagrams can be enhanced by factors of M^2/m_μ^2 relative to the 1-loop diagrams, where M is a heavy Higgs or heavy fermion mass. For completeness, these results are given in Appendix C.

In Figs. 16 and 17, we show the contributions to Δa_μ in the 2HDM for relatively heavy $m_{2,3}$ and m_{H^+} in units of 10^{-11} . For $|\sin \alpha_b| \lesssim 0.5$, there is almost no sensitivity to the CP violating phase. The largest contribution is found in the Type-II model for large $\tan \beta$ and is of opposite sign to that needed to explain the discrepancy of Eq. (4.9).

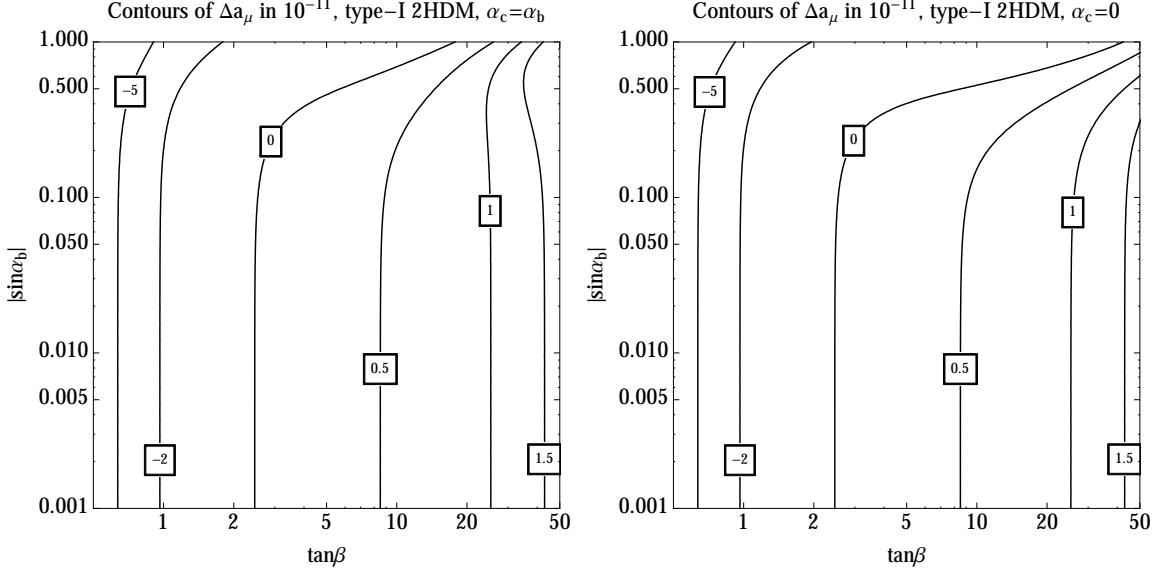


Figure 16. Contributions to $(g-2)_\mu$ in the CP violating Type-I 2HDM from the Barr-Zee diagrams. The heavy scalar masses are fixed to be $m_{h_2} = 400$ GeV, $m_{h_3} = 450$ GeV, $m_{H^+} = 420$ GeV, and the model parameter $\nu = 1$.

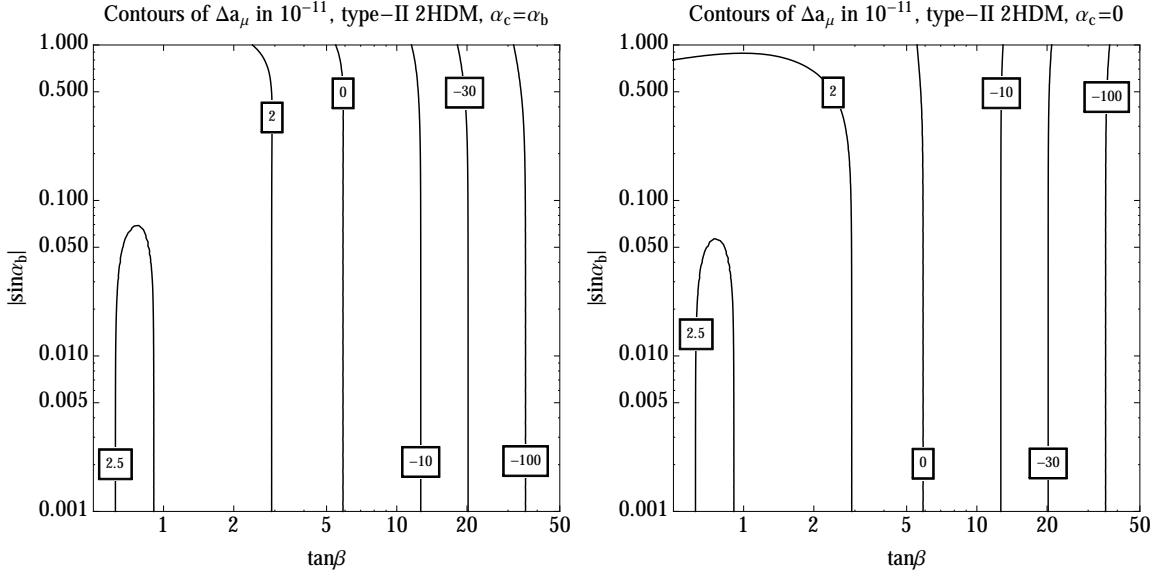


Figure 17. Similar to Fig. 16 but for Type-II 2HDM.

5 Conclusion

The CP mixture of the 126 GeV Higgs boson is an important property of the Higgs sector that deserves further scrutiny. A non-zero CP component is theoretically well motivated and may be the origin of the cosmic baryon asymmetry. An important consequence of the 126 GeV Higgs boson having a sizable CP odd mixture is that the new physics responsible for this cannot be decoupled and must lie near the electroweak scale.

In the context of CP violating, flavor conserving two-Higgs-doublet models, we studied the impact of the heavy Higgs searches at the LHC on the CP violating parameters. In this class of models, CP violation appears in the neutral Higgs sector, where there are two more real scalars ($h_{2,3}$) in addition to the lightest 126 GeV one. The couplings of the heavy Higgs scalars with electroweak gauge bosons are very sensitive to the CP violation in the Higgs sector. Turning on a CP odd mixture in the 126 GeV Higgs boson will also turn on the heavy Higgs decay channels into gauge bosons, $h_{2,3} \rightarrow WW/ZZ$ and Zh_1 . There is data from the LHC from the search for a SM like Higgs boson in these decay channels, and the non-discovery of a heavy Higgs can be re-interpreted as constraints on the allowed deviation from the alignment limit in the two-Higgs-doublet models without CP violation.

In this work, we point out that heavy Higgs searches are also extremely useful for constraining Higgs sector CP violation and in particular the CP mixture of the 126 GeV Higgs boson. We demonstrate that the constraints from heavy Higgs searches are largely complementary to the low energy EDM constraints. We compare our results with the limits from the global fit to the 126 GeV Higgs data, and find they can place much stronger limits than the light Higgs coupling fit, especially in the interesting regions when there are destructive contributions to the EDM. We find in these regions that the heavy Higgs searches are at the frontier of probing Higgs sector CP violation. The current limit on the CP violating mixing angle, parametrized by α_b , is constrained to be less than 30%, and the LHC heavy Higgs search can further narrow down the angle to less than a 10% level with the high luminosity runs. We also expect our work to be a roadmap for the future searches for Higgs sector CP violation and the exciting interplay across various experimental frontiers.

For completeness, we have also explored other relevant constraints from electroweak oblique parameters, the muon $g - 2$ and from B physics, and discussed their implications on the heavy Higgs parameter limits in CP violating 2HDMs.

A Solving the potential parameters in the approximate Z_2 case

In this section, we list the relations between the potential parameters and the phenomenological parameters listed in Eq. (2.3) in the approximate Z_2 symmetric 2HDMs.

$$m_{11}^2 = \lambda_1 v^2 \cos^2 \beta + (\lambda_3 + \lambda_4) v^2 \sin^2 \beta - \text{Re}(m_{12}^2 e^{i\xi}) \tan \beta + \text{Re}(\lambda_5 e^{2i\xi}) v^2 \sin^2 \beta, \quad (\text{A.1})$$

$$m_{22}^2 = \lambda_2 v^2 \sin^2 \beta + (\lambda_3 + \lambda_4) v^2 \cos^2 \beta - \text{Re}(m_{12}^2 e^{i\xi}) \cot \beta + \text{Re}(\lambda_5 e^{2i\xi}) v^2 \cos^2 \beta, \quad (\text{A.2})$$

$$\text{Im}(m_{12}^2) = v^2 \sin \beta \cos \beta \text{Im}(\lambda_5), \quad (\text{A.3})$$

$$\lambda_1 = \frac{m_{h_1}^2 \sin^2 \alpha \cos^2 \alpha_b + m_{h_2}^2 R_{21}^2 + m_{h_3}^2 R_{31}^2}{v^2 \cos \beta^2} - \nu \tan^2 \beta, \quad (\text{A.4})$$

$$\lambda_2 = \frac{m_{h_1}^2 \cos^2 \alpha \cos^2 \alpha_b + m_{h_2}^2 R_{22}^2 + m_{h_3}^2 R_{32}^2}{v^2 \sin \beta^2} - \nu \cot^2 \beta, \quad (\text{A.5})$$

$$\lambda_4 = 2\nu - \text{Re}\lambda_5 - \frac{2m_{H^+}^2}{v^2}, \quad (\text{A.6})$$

$$\lambda_3 = \nu - \frac{m_{h_1}^2 \sin \alpha \cos \alpha \cos^2 \alpha_b - m_{h_2}^2 R_{21} R_{22} - m_{h_3}^2 R_{31} R_{32}}{v^2 \sin \beta \cos \beta} - \lambda_4 - \text{Re}\lambda_5, \quad (\text{A.7})$$

$$\text{Re}\lambda_5 = \nu - \frac{m_{h_1}^2 \sin^2 \alpha_b + \cos^2 \alpha_b (m_{h_2}^2 \sin^2 \alpha_c + m_{h_3}^2 \cos^2 \alpha_c)}{v^2}, \quad (\text{A.8})$$

$$\begin{aligned} \text{Im}\lambda_5 = \frac{2 \cos \alpha_b}{v^2 \sin \beta} & \left[(m_{h_2}^2 - m_{h_3}^2) \cos \alpha \sin \alpha_c \cos \alpha_c \right. \\ & \left. + (m_{h_1}^2 - m_{h_2}^2 \sin^2 \alpha_c - m_{h_3}^2 \cos^2 \alpha_c) \sin \alpha \sin \alpha_b \right]. \end{aligned} \quad (\text{A.9})$$

There is an additional constraint,

$$\tan \beta = \frac{(m_{h_2}^2 - m_{h_3}^2) \cos \alpha_c \sin \alpha_c + (m_{h_1}^2 - m_{h_2}^2 \sin^2 \alpha_c - m_{h_3}^2 \cos^2 \alpha_c) \tan \alpha \sin \alpha_b}{(m_{h_2}^2 - m_{h_3}^2) \tan \alpha \cos \alpha_c \sin \alpha_c - (m_{h_1}^2 - m_{h_2}^2 \sin^2 \alpha_c - m_{h_3}^2 \cos^2 \alpha_c) \sin \alpha_b}. \quad (\text{A.10})$$

B Tri-linear Higgs Couplings

From the quartic terms in the scalar potential Eq. (2.1), we can obtain the interactions between three neutral scalars, in the basis of (H_1^0, H_2^0, A^0) ,

$$\begin{aligned} \mathcal{L}_{3s} = & \frac{1}{4} (A^0)^3 \cos \beta \left\{ 2 \sin \beta \text{Im}\lambda_5 - \cos \beta \text{Im}\lambda_7 \right\} \\ & + \frac{1}{8} (A^0)^2 \left\{ \left[-5H_1^0 \cos \beta + H_1^0 \cos(3\beta) - H_2^0 (5 \sin \beta + \sin(3\beta)) \right] \text{Re}\lambda_5 \right. \\ & \quad \left. + 4 \left[H_1^0 \cos \beta \sin^2 \beta \lambda_1 + H_2^0 \cos^2 \beta \sin \beta \lambda_2 + (H_1^0 \cos^3 \beta + H_2^0 \sin^3 \beta) (\lambda_3 + \lambda_4) \right] \right\} \\ & + \frac{1}{4} A^0 \left\{ \left[4H_1^0 H_2^0 + ((H_1^0)^2 + (H_2^0)^2) \sin(2\beta) \right] \text{Im}\lambda_5 + H_2^0 (2H_2^0 - H_2^0 \cos(2\beta) + H_1^0 \sin(2\beta)) \text{Im}\lambda_7 \right\} \\ & + \frac{1}{2} \left\{ H_2^0 \sin \beta \left[(H_2^0)^2 \lambda_2 + (H_1^0)^2 (\lambda_3 + \lambda_4 + \text{Re}\lambda_5) \right] + H_1^0 \cos \beta \left[(H_1^0)^2 \lambda_1 + (H_2^0)^2 (\lambda_3 + \lambda_4 + \text{Re}\lambda_5) \right] \right\}. \end{aligned} \quad (\text{B.1})$$

From these terms one can readily obtain the $h_i h_j h_k$ interactions in the mass eigenstate basis (h_1, h_2, h_3) using the orthogonal matrix R from Eq. (2.4). In particular, the g_{i11} ($i = 2, 3$) coefficients used in Eq. (2.24) are

$$g_{i11} = \frac{1}{2} \sum_{a \leq b \leq c} \frac{\partial^3 \mathcal{L}_{3s}}{\partial H_a \partial H_b \partial H_c} \frac{\partial H_a}{\partial h_1} \frac{\partial H_b}{\partial h_1} \frac{\partial H_c}{\partial h_i} = \frac{1}{2} \sum_{a \leq b \leq c} \frac{\partial^3 \mathcal{L}_{3s}}{\partial H_a \partial H_b \partial H_c} R_{1a} R_{1b} R_{ic}, \quad (\text{B.2})$$

where $\{H_a\} = (H_1^0, H_2^0, A^0)$.

C Formula for $g - 2$

The magnetic and electric dipole moments of a fermion f correspond to the real and imaginary parts of the Wilson coefficient c of the effective operator

$$\mathcal{L}_{eff} = c \bar{f}_L \sigma_{\mu\nu} f_R F^{\mu\nu} + \text{h.c.}, \quad (\text{C.1})$$

where in the Type-I and Type-II 2HDMs we consider the main contributions to the coefficient c that arise from the two-loop Barr-Zee type diagrams. It is straightforward to translate the electron EDM results to the corresponding muon anomalous dipole moment. The prescription for the translation is,

$$a_\mu = \frac{2m_\mu^2}{eQ_\mu m_e} \times \begin{cases} d_e^\gamma \begin{pmatrix} c_e \rightarrow \tilde{c}_\mu \\ \tilde{c}_e \rightarrow -c_\mu \end{pmatrix}, & h\gamma\gamma, hZ\gamma \text{ diagrams} \\ d_e^\gamma \begin{pmatrix} \text{Im}(a_{W^+H^-h_i}) \rightarrow -\text{Re}(a_{W^+H^-h_i}) \end{pmatrix}, & W^\pm H_\mp \gamma \text{ diagrams (S)} \\ d_e^\gamma \begin{pmatrix} \text{Im}(c_{\tilde{t}_R b_L H^+}^* c_{\tilde{\nu}_e R H^+}) \\ \rightarrow -\text{Re}(c_{\tilde{t}_R b_L H^+}^* c_{\tilde{\nu}_e R H^+}) \end{pmatrix}, & W^\pm H_\mp \gamma \text{ diagrams (F)} \end{cases} \quad (\text{C.2})$$

where $AB\gamma$ corresponds to those Barr-Zee diagrams with h_1 lines connected to the upper loop, and the S/F in the bracket corresponds to heavy Higgs scalars/SM fermions running in the upper loop. The $h\gamma\gamma, hZ\gamma$ and $W^\pm H_\mp \gamma$ diagram (S) contributions to the EDM have been summarized in Refs. [10, 71]. The $W^\pm H_\mp \gamma$ diagram (F) contributions to the EDM vanish in 2HDMs with approximate Z_2 symmetry, but have been calculated in a more general framework in Ref. [72]. We perform the above translation based on results in Ref. [72]. See also Ref. [73] for a recent work on $g - 2$ in a 2HDM.

We list below the analytic results for the contributions to the muon $g - 2$ in a 2HDM:

$$\begin{aligned}
(\Delta a_\mu)_f^{h\gamma\gamma} &= \frac{G_F m_\mu^2 N_c Q_f^2 \alpha}{2\sqrt{2}\pi^3} \sum_{i=1}^3 \left[-c_{f,i} c_{\mu,i} f(z_f^i) + \tilde{c}_{f,i} \tilde{c}_{\mu,i} g(z_f^i) \right] , \\
(\Delta a_\mu)_f^{hZ\gamma} &= \frac{G_F m_\mu^2 N_c Q_t g_{Z\bar{e}e}^V g_{Z\bar{f}f}^V}{8\sqrt{2}\pi^4 Q_\mu} \sum_{i=1}^3 \left[-c_{f,i} c_{\mu,i} \tilde{f}\left(z_f^i, \frac{m_f^2}{M_Z^2}\right) + \tilde{c}_{f,i} \tilde{c}_{\mu,i} \tilde{g}\left(z_f^i, \frac{m_f^2}{M_Z^2}\right) \right] , \\
(\Delta a_\mu)_W^{h\gamma\gamma} &= \frac{G_F m_\mu^2 \alpha}{8\sqrt{2}\pi^3} \sum_{i=1}^3 \left[\left(6 + \frac{1}{z_w^i}\right) f(z_w^i) + \left(10 - \frac{1}{z_w^i}\right) g(z_w^i) \right] (-c_{\mu,i}) a_i , \\
(\Delta a_\mu)_W^{hZ\gamma} &= \frac{g_{Z\bar{f}f}^V g_{ZWW}}{Q_\mu} \frac{G_F m_\mu^2}{32\sqrt{2}\pi^4} \sum_{i=1}^3 \left[\left(6 - \sec^2 \theta_W + \frac{2 - \sec^2 \theta_W}{2z_w^i}\right) \tilde{f}(z_w^i, \cos^2 \theta_W) \right. \\
&\quad \left. + \left(10 - 3 \sec^2 \theta_W - \frac{2 - \sec^2 \theta_W}{2z_w^i}\right) \tilde{g}(z_w^i, \cos^2 \theta_W) \right] (-c_{\mu,i}) a_i , \\
(\Delta a_\mu)_{H^+}^{h\gamma\gamma} &= \frac{G_F m_\mu^2 \alpha}{8\sqrt{2}\pi^3} \left(\frac{v}{m_{H^+}}\right)^2 \sum_{i=1}^3 \left[f(z_H^i) - g(z_H^i) \right] (-c_{\mu,i}) \bar{\lambda}_i \\
(\Delta a_\mu)_{H^+}^{hZ\gamma} &= \frac{g_{Z\bar{f}f}^V g_{ZH^+H^-}}{Q_\mu} \frac{G_F m_\mu^2}{32\sqrt{2}\pi^4} \left(\frac{v}{m_{H^+}}\right)^2 \sum_{i=1}^3 \left[\tilde{f}(z_H^i, m_{H^+}^2/M_Z^2) - \tilde{g}(z_H^i, m_{H^+}^2/M_Z^2) \right] (-c_{\mu,i}) \bar{\lambda}_i , \\
(\Delta a_\mu)_H^{HW\gamma} &= -\frac{G_F m_\mu^2 c_{H^+\bar{\nu}e^-}}{64\sqrt{2}\pi^4 Q_\mu} \sum_i \left[\frac{e^2}{2\sin^2 \theta_W} \mathcal{I}_4(m_{h_i}^2, m_{H^+}^2) a_i - \mathcal{I}_5(m_{h_i}^2, m_{H^+}^2) \bar{\lambda}_i \right] (-\text{Re}(a_{W^+H^-h_i})) , \\
(\Delta a_\mu)_{t,b}^{HW\gamma} &= \left(\frac{3g^2}{16\pi^2}\right) \left(\frac{g^2 m_\mu^2}{32\pi^2 M_W^2}\right) (-\text{Re}(c_{\bar{t}RbLH^+}^* c_{H^+\bar{\nu}e^-})) \left(\frac{2}{3} F_t - \frac{1}{3} F_b\right) , \tag{C.3}
\end{aligned}$$

where $z_f^i = m_f^2/m_{h_i}^2$ ($f = t, b$), $z_w^i = M_W^2/m_{h_i}^2$, $z_H^i = m_{H^+}^2/m_{h_i}^2$, and $c_{e,i} = c_{\mu,i} = c_{\tau,i}$, $\tilde{c}_{e,i} = \tilde{c}_{\mu,i} = \tilde{c}_{\tau,i}$ can be obtained from Table 1.

The relevant coefficients are,

$$\begin{aligned}
g_{Z\bar{f}f}^V &= \frac{g}{2\cos\theta_W} \left(T_3^f - 2Q^f \sin^2\theta_W\right) , \\
g_{WWZ} &= e \cot\theta_W , \\
g_{ZH^+H^-} &= \frac{1}{2} e \cot\theta_W (1 - \tan^2\theta_W) , \\
\bar{\lambda}_i &= R_{i1} \cdot (\lambda_3 \cos^2\beta + (\lambda_1 - \lambda_4 - \text{Re}\lambda_5) \sin^2\beta) \cos\beta \\
&\quad + R_{i2} \cdot (\lambda_3 \sin^2\beta + (\lambda_2 - \lambda_4 - \text{Re}\lambda_5) \cos^2\beta) \sin\beta \\
&\quad + R_{i3} \cdot \text{Im}\lambda_5 \sin\beta \cos\beta , \\
a_{W^+H^-h_i} &= -\sin\beta R_{i1} + \cos\beta R_{i2} + iR_{i3} , \\
c_{\bar{t}RbLH^+} &= \cot\beta , \\
c_{H^+\bar{\nu}e^-} &= \begin{cases} \cot\beta & \text{Type I} \\ -\tan\beta & \text{Type II} \end{cases} \tag{C.4}
\end{aligned}$$

The relevant loop functions are,

$$\begin{aligned}
h_0(z) &= \frac{z^4}{2} \int_0^1 dx \int_0^1 dy \frac{x^3 y^3 (1-x)}{(z^2 x(1-xy) + (1-y)(1-x))^2} , \\
f(z) &= \frac{z}{2} \int_0^1 dx \frac{1-2x(1-x)}{x(1-x)-z} \log \frac{x(1-x)}{z} , \\
g(z) &= \frac{z}{2} \int_0^1 dx \frac{1}{x(1-x)-z} \log \frac{x(1-x)}{z} , \\
h(z) &= \frac{z}{2} \int_0^1 dx \frac{1}{z-x(1-x)} \left(1 + \frac{z}{z-x(1-x)} \log \frac{x(1-x)}{z} \right) , \\
\tilde{f}(x, y) &= \frac{yf(x)}{y-x} + \frac{xf(y)}{x-y} , \\
\tilde{g}(x, y) &= \frac{yg(x)}{y-x} + \frac{xg(y)}{x-y} , \\
\mathcal{I}_{4,5}(m_1^2, m_2^2) &= \frac{M_W^2}{m_{H^+}^2 - M_W^2} (I_{4,5}(M_W^2, m_1^2) - I_{4,5}(m_2^2, m_1^2)) , \\
I_4(m_1^2, m_2^2) &= \int_0^1 dz (1-z)^2 \left(z - 4 + z \frac{m_{H^+}^2 - m_2^2}{M_W^2} \right) \\
&\quad \times \frac{m_1^2}{M_W^2(1-z) + m_2^2 z - m_1^2 z(1-z)} \log \frac{M_W^2(1-z) + m_2^2 z}{m_1^2 z(1-z)} , \\
I_5(m_1^2, m_2^2) &= \int_0^1 dz \frac{m_1^2 z(1-z)^2}{M_{H^+}^2(1-z) + m_2^2 z - m_1^2 z(1-z)} \log \frac{M_{H^+}^2(1-z) + m_2^2 z}{m_1^2 z(1-z)} , \\
Sp(z) &= - \int_0^z t^{-1} \ln(1-t) dt , \\
T(z) &= \frac{1-3z}{z^2} \frac{\pi^2}{6} - \left(\frac{1}{z} - \frac{5}{2} \right) \ln z - \frac{1}{z} - \left(2 - \frac{1}{z} \right) \left(1 - \frac{1}{z} \right) Sp(1-z) , \\
B(z) &= \frac{1}{z} + \frac{2z-1}{z^2} \frac{\pi^2}{6} + \left(\frac{3}{2} - \frac{1}{z} \right) \ln z - \left(2 - \frac{1}{z} \right) \frac{1}{z} Sp(1-z) , \\
F_t &= \frac{T(m_{H^+}^2/m_t^2) - T(M_W^2/m_t^2)}{m_{H^+}^2/m_t^2 - M_W^2/m_t^2} , \\
F_b &= \frac{B(m_{H^+}^2/m_t^2) - B(M_W^2/m_t^2)}{m_{H^+}^2/m_t^2 - M_W^2/m_t^2} . \tag{C.5}
\end{aligned}$$

Acknowledgements

We thank Jing Shu and Michael Spira for useful discussions. The work of C.-Y. Chen and S. Dawson is supported by the U.S. Department of Energy under grant No. DE-AC02-98CH10886 and contract DE-AC02-76SF00515. This work of Y. Zhang is supported by the Gordon and Betty Moore Foundation through Grant #776 to the Caltech Moore Center for Theoretical Cosmology and Physics, and by the DOE Grant DE-FG02-92ER40701, and also by a DOE Early Career Award under Grant No. DE-SC0010255.

References

- [1] G. Aad *et al.* [ATLAS Collaboration], Phys. Lett. B **716**, 1 (2012) [arXiv:1207.7214 [hep-ex]].
- [2] S. Chatrchyan *et al.* [CMS Collaboration], Phys. Lett. B **716**, 30 (2012) [arXiv:1207.7235 [hep-ex]].
- [3] G. C. Branco, P. M. Ferreira, L. Lavoura, M. N. Rebelo, M. Sher and J. P. Silva, Phys. Rept. **516**, 1 (2012) [arXiv:1106.0034 [hep-ph]].
- [4] The ATLAS collaboration, ATLAS-CONF-2014-010, ATLAS-COM-CONF-2014-011.
- [5] C. Y. Chen and S. Dawson, Phys. Rev. D **87**, 055016 (2013) [arXiv:1301.0309 [hep-ph]].
- [6] B. Coleppa, F. Kling and S. Su, JHEP **1401**, 161 (2014) [arXiv:1305.0002 [hep-ph]].
- [7] K. Cheung, J. S. Lee and P. Y. Tseng, JHEP **1401**, 085 (2014) [arXiv:1310.3937 [hep-ph]].
- [8] J. Shu and Y. Zhang, Phys. Rev. Lett. **111**, no. 9, 091801 (2013) [arXiv:1304.0773 [hep-ph]].
- [9] D. E. Morrissey and M. J. Ramsey-Musolf, New J. Phys. **14**, 125003 (2012) [arXiv:1206.2942 [hep-ph]].
- [10] S. Inoue, M. J. Ramsey-Musolf and Y. Zhang, Phys. Rev. D **89** (2014) 11, 115023 [arXiv:1403.4257 [hep-ph]].
- [11] J. Brod, U. Haisch and J. Zupan, JHEP **1311**, 180 (2013) [arXiv:1310.1385 [hep-ph], arXiv:1310.1385].
- [12] D. Fontes, J. C. Romo, R. Santos and J. P. Silva, arXiv:1502.01720 [hep-ph].
- [13] L. Lavoura and J. P. Silva, Phys. Rev. D **50**, 4619 (1994) [hep-ph/9404276].
- [14] A. Barroso, P. M. Ferreira, R. Santos and J. P. Silva, Phys. Rev. D **86**, 015022 (2012) [arXiv:1205.4247 [hep-ph]].
- [15] V. Khachatryan *et al.* [CMS Collaboration], arXiv:1411.3441 [hep-ex].
- [16] The ATLAS Collaboration, ATLAS-CONF-2013-013.
- [17] R. Harnik, A. Martin, T. Okui, R. Primulando and F. Yu, Phys. Rev. D **88**, no. 7, 076009 (2013) [arXiv:1308.1094 [hep-ph]].
- [18] F. Bishara, Y. Grossman, R. Harnik, D. J. Robinson, J. Shu and J. Zupan, JHEP **1404**, 084 (2014) [arXiv:1312.2955 [hep-ph]].
- [19] Y. Chen, A. Falkowski, I. Low and R. Vega-Morales, Phys. Rev. D **90**, 113006 (2014) [arXiv:1405.6723 [hep-ph]].
- [20] M. J. Dolan, P. Harris, M. Jankowiak and M. Spannowsky, Phys. Rev. D **90**, no. 7, 073008 (2014) [arXiv:1406.3322 [hep-ph]].
- [21] S. Berge, W. Bernreuther and S. Kirchner, Eur. Phys. J. C **74**, no. 11, 3164 (2014) [arXiv:1408.0798 [hep-ph]].
- [22] X. G. He, G. N. Li and Y. J. Zheng, arXiv:1501.00012 [hep-ph].
- [23] S. Bar-Shalom, D. Atwood, G. Eilam, R. R. Mendel and A. Soni, Phys. Rev. D **53**, 1162 (1996) [hep-ph/9508314].
- [24] D. Atwood, S. Bar-Shalom, G. Eilam and A. Soni, Phys. Rept. **347**, 1 (2001) [hep-ph/0006032].

- [25] S. Ipek, Phys. Rev. D **89**, 073012 (2014) [arXiv:1310.6790 [hep-ph]].
- [26] K. Cheung, J. S. Lee, E. Senaha and P. Y. Tseng, JHEP **1406**, 149 (2014) [arXiv:1403.4775 [hep-ph]].
- [27] L. Bian, T. Liu and J. Shu, arXiv:1411.6695 [hep-ph].
- [28] M. S. Carena, J. R. Ellis, S. Mrenna, A. Pilaftsis and C. E. M. Wagner, Nucl. Phys. B **659**, 145 (2003) [hep-ph/0211467].
- [29] P. Bechtle, O. Brein, S. Heinemeyer, O. Stl, T. Stefaniak, G. Weiglein and K. E. Williams, Eur. Phys. J. C **74**, no. 3, 2693 (2014) [arXiv:1311.0055 [hep-ph]].
- [30] A. Arbey, J. Ellis, R. M. Godbole and F. Mahmoudi, arXiv:1410.4824 [hep-ph].
- [31] B. Li and C. E. M. Wagner, arXiv:1502.02210 [hep-ph].
- [32] A. Chakraborty, B. Das, J. L. Diaz-Cruz, D. K. Ghosh, S. Moretti and P. Poulose, Phys. Rev. D **90**, no. 5, 055005 (2014) [arXiv:1301.2745 [hep-ph]].
- [33] M. Carena, H. E. Haber, I. Low, N. R. Shah and C. E. M. Wagner, Phys. Rev. D **91**, no. 3, 035003 (2015) [arXiv:1410.4969 [hep-ph]].
- [34] C. Y. Chen, S. Dawson and M. Sher, Phys. Rev. D **88**, 015018 (2013) [arXiv:1305.1624 [hep-ph]].
- [35] N. Craig, J. Galloway and S. Thomas, arXiv:1305.2424 [hep-ph].
- [36] A. Freitas and P. Schwaller, Phys. Rev. D **87**, no. 5, 055014 (2013) [arXiv:1211.1980 [hep-ph]].
- [37] A. Djouadi and G. Moreau, Eur. Phys. J. C **73**, no. 9, 2512 (2013) [arXiv:1303.6591 [hep-ph]].
- [38] W. F. Chang, W. P. Pan and F. Xu, Phys. Rev. D **88**, no. 3, 033004 (2013) [arXiv:1303.7035 [hep-ph]].
- [39] A. J. Buras, G. Isidori and P. Paradisi, Phys. Lett. B **694**, 402 (2011) [arXiv:1007.5291 [hep-ph]].
- [40] J. M. Cline, K. Kainulainen and M. Trott, JHEP **1111**, 089 (2011) [arXiv:1107.3559 [hep-ph]].
- [41] M. Jung and A. Pich, arXiv:1308.6283 [hep-ph].
- [42] S. Dittmaier *et al.* [LHC Higgs Cross Section Working Group Collaboration], arXiv:1101.0593 [hep-ph].
- [43] <https://twiki.cern.ch/twiki/bin/view/LHCPhysics/CrossSections>
- [44] S. Heinemeyer *et al.* [LHC Higgs Cross Section Working Group Collaboration], arXiv:1307.1347 [hep-ph].
- [45] <http://tiger.web.psi.ch/grids/>
- [46] F. Maltoni, G. Ridolfi and M. Ubiali, JHEP **1207**, 022 (2012) [JHEP **1304**, 095 (2013)] [arXiv:1203.6393 [hep-ph]].
- [47] [ATLAS Collaboration], ATLAS-CONF-2013-027, ATLAS-COM-CONF-2013-005.
- [48] S. Chatrchyan *et al.* [CMS Collaboration], Eur. Phys. J. C **73**, no. 6, 2469 (2013) [arXiv:1304.0213 [hep-ex]]. CMS-HIG-12-034.
- [49] The ATLAS collaboration, ATLAS-CONF-2013-067, ATLAS-COM-CONF-2013-082.

- [50] The CMS Collaboration, CMS-HIG-14-011.
- [51] G. Aad *et al.* [ATLAS Collaboration], arXiv:1502.04478 [hep-ex].
- [52] V. Khachatryan *et al.* [CMS Collaboration], JHEP **1410**, 160 (2014) [arXiv:1408.3316 [hep-ex]]. CMS-HIG-13-021.
- [53] A. Djouadi and J. Quevillon, JHEP **1310**, 028 (2013) [arXiv:1304.1787 [hep-ph]].
- [54] The CMS Collaboration, CMS-HIG-14-009.
- [55] G. Aad *et al.* [ATLAS Collaboration], arXiv:1412.2641 [hep-ex].
- [56] The ATLAS Collaboration, ATLAS-CONF-2014-009.
- [57] G. Aad *et al.* [ATLAS Collaboration], Phys. Rev. D **90**, no. 11, 112015 (2014) [arXiv:1408.7084 [hep-ex]].
- [58] The ATLAS Collaboration, ATLAS-CONF-2013-079.
- [59] G. Aad *et al.* [ATLAS Collaboration], arXiv:1501.04943 [hep-ex].
- [60] J. Engel, M. J. Ramsey-Musolf and U. van Kolck, Prog. Part. Nucl. Phys. **71**, 21 (2013) [arXiv:1303.2371 [nucl-th]].
- [61] C. Y. Chen, arXiv:1308.3487 [hep-ph].
- [62] P. M. Ferreira, J. F. Guion, H. E. Haber and R. Santos, Phys. Rev. D **89**, no. 11, 115003 (2014) [arXiv:1403.4736 [hep-ph]].
- [63] F. Mahmoudi and O. Stal, Phys. Rev. D **81**, 035016 (2010) [arXiv:0907.1791 [hep-ph]].
- [64] A. Wahab El Kaffas, P. Osland and O. M. Ogreid, Phys. Rev. D **76**, 095001 (2007) [arXiv:0706.2997 [hep-ph]].
- [65] W. Grimus, L. Lavoura, O. M. Ogreid and P. Osland, Nucl. Phys. B **801**, 81 (2008) [arXiv:0802.4353 [hep-ph]].
- [66] H. J. He, N. Polonsky and S. f. Su, Phys. Rev. D **64**, 053004 (2001) [hep-ph/0102144].
- [67] H. E. Haber and D. O’Neil, Phys. Rev. D **83**, 055017 (2011) [arXiv:1011.6188 [hep-ph]].
- [68] R. Barbieri, L. J. Hall and V. S. Rychkov, Phys. Rev. D **74**, 015007 (2006) [hep-ph/0603188].
- [69] M. Baak *et al.* [Gfitter Group Collaboration], Eur. Phys. J. C **74**, 3046 (2014) [arXiv:1407.3792 [hep-ph]].
- [70] M. Davier and W. J. Marciano, Ann. Rev. Nucl. Part. Sci. **54**, 115 (2004).
- [71] T. Abe, J. Hisano, T. Kitahara and K. Tobioka, JHEP **1401**, 106 (2014) [arXiv:1311.4704 [hep-ph], arXiv:1311.4704].
- [72] D. Bowser-Chao, D. Chang and W. Y. Keung, Phys. Rev. Lett. **79**, 1988 (1997) [hep-ph/9703435].
- [73] V. Ilisie, arXiv:1502.04199 [hep-ph].